

MICROCOPY RESOLUTION TEST CHART  
NATIONAL BUREAU OF STANDARDS-1963-A

2

AD-A156 008

OPTIMAL ESTIMATION OF A HIGH DEGREE GRAVITY FIELD FROM A GLOBAL SET OF 1°x 1° ANOMALIES TO DEGREE AND ORDER 250

D.P. Hajela

The Ohio State University  
Research Foundation  
Columbus, Ohio 43212

August 1984

Scientific Report No. 7

Approved for public release; distribution unlimited

AIR FORCE GEOPHYSICS LABORATORY  
AIR FORCE SYSTEMS COMMAND  
UNITED STATES AIR FORCE  
HANSCOM AFB, MASSACHUSETTS 01731

DTIC  
ELECTE  
JUN 26 1985  
S D  
B

DTIC FILE COPY

85 06 10 10 3

CONTRACTOR REPORTS

This technical report has been reviewed and is approved for publication.

  
CHRISTOPHER JEKELI  
Contract Manager

  
THOMAS P. ROONEY  
Chief, Geodesy & Gravity Branch

FOR THE COMMANDER

  
DONALD H. ECKHARDT  
Director  
Earth Sciences Division

This report has been reviewed by the ESD Public Affairs Office (PA) and is releasable to the National Technical Information Service (NTIS).

Qualified requesters may obtain additional copies from the Defense Technical Information Center. All others should apply to the National Technical Information Service.

If your address has changed, or if you wish to be removed from the mailing list, or if the addressee is no longer employed by your organization, please notify AFGL/DAA, Hanscom AFB, MA 01731. This will assist us in maintaining a current mailing list.

unclassified

SECURITY CLASSIFICATION OF THIS PAGE (When Data Entered)

REPORT DOCUMENTATION PAGE		READ INSTRUCTIONS BEFORE COMPLETING FORM
1. REPORT NUMBER AFGL-TR-84-0263	2. GOVT ACCESSION NO.	3. RECIPIENT'S CATALOG NUMBER
4. TITLE (and Subtitle) OPTIMAL ESTIMATION OF A HIGH DEGREE GRAVITY FIELD FROM A GLOBAL SET OF 1°x 1° ANOMALIES TO DEGREE AND ORDER 250	5. TYPE OF REPORT & PERIOD COVERED Scientific Report No. 7	
	6. PERFORMING ORG. REPORT NUMBER OSU/DGSS-358	
7. AUTHOR(s) D.P. Hajela	8. CONTRACT OR GRANT NUMBER(s) F19628-82-X-0022	
9. PERFORMING ORGANIZATION NAME AND ADDRESS The Ohio State University Research Foundation 1958 Neil Avenue, Columbus, OH 43210	10. PROGRAM ELEMENT, PROJECT, TASK AREA & WORK UNIT NUMBERS 61102F 2309G1BC	
11. CONTROLLING OFFICE NAME AND ADDRESS Air Force Geophysics Laboratory Hanscom AFB, Massachusetts 01730 Monitor/Christopher Jekeli/LWG	12. REPORT DATE August 1984	
	13. NUMBER OF PAGES 68	
14. MONITORING AGENCY NAME & ADDRESS (if different from Controlling Office)	15. SECURITY CLASS. (of this report) Unclassified	
	15a. DECLASSIFICATION/DOWNGRADING SCHEDULE	
16. DISTRIBUTION STATEMENT (of this Report)  Approved for public release; distribution unlimited		
17. DISTRIBUTION STATEMENT (of the abstract entered in Block 20, if different from Report)		
18. SUPPLEMENTARY NOTES		
19. KEY WORDS (Continue on reverse side if necessary and identify by block number)  Earth's Gravity Field, Spherical Harmonics, Degree and Order 250, Optimal Estimation. <i>1 by 1 deg</i>		
20. ABSTRACT (Continue on reverse side if necessary and identify by block number)  An algorithm developed by Colombo (1981) for the optimal estimation of potential coefficients has been implemented with global 1°x 1° gravity anomalies. The reformulation of the algorithm, and the modifications, have been described. The effect of changes in anomaly error estimates, and change in the anomaly data, on the optimally estimated potential coefficients has been examined.		

unclassified

SECURITY CLASSIFICATION OF THIS PAGE (When Data Entered)

unclassified

SECURITY CLASSIFICATION OF THIS PAGE(When Data Entered)

4-9 → Potential coefficients were estimated complete to degree and order 250 with present realistic anomaly error estimates, and also with idealized anomaly error estimates. A comparison with the current set of potential coefficients (Rapp, 1981) complete to degree and order 180 shows a realistic coefficient percentage improvement of about 8% at degree 60, increasing to about 33% at degree 180. The cumulative undulation and anomaly difference to degree 180 is 1.51 meters and 2.7 mgals respectively. The present coefficient error estimates are better by a factor of about two when compared to the current coefficient error estimates. → cont. key words include: sea level

In the optimally estimated potential coefficients from  $1^{\circ} \times 1^{\circ}$  anomalies, the undulation and anomaly magnitudes per degree decrease to about 1 cm and 0.5 mgals respectively near degree 250. The coefficient percentage error per degree exceeds 80% near degree 250. A global set of  $30' \times 30'$  gravity anomalies would be needed for estimating the potential coefficients beyond degree 250.

unclassified

SECURITY CLASSIFICATION OF THIS PAGE(When Data Entered)

### Foreword

This report was prepared by Dhaneshwar P. Hajela, Associate Professor, Department of Geodetic Science and Surveying, The Ohio State University, under Air Force Contract No. F19628-82-K-0022, The Ohio State University Research Foundation Project No. 714274. The contract covering this research is administered by the Air Force Geophysics Laboratory, Hanscom Air Force Base, Massachusetts, with Dr. Christopher Jekeli, Scientific Program Officer.

Accession For	
DTIC GRA&I	<input checked="" type="checkbox"/>
DTIC TAB	<input type="checkbox"/>
Unannounced	<input type="checkbox"/>
Justification	
By	
Distribution/	
Availability Codes	
Dist	Avail and/or Special
A-1	



### Acknowledgements

I am thankful to Richard H. Rapp for his advice and support of this study. The original credit for the formulation and programming of the optimal estimation procedure belongs to Oscar Colombo. Helpful discussions are acknowledged with Rene' Forsberg and John Snowden. Laura Brumfield's assistance in the careful typing of this report is sincerely appreciated.

## Table of Contents

Foreword	iii
Acknowledgements	iv
List of Figures	vi
List of Tables	vii
1. Introduction	1
2. Harmonic Analysis and Synthesis	4
2.1 Quadrature Formulas with De-smoothing Factors	4
2.2 Quadrature Formulas with Optimal Weights	6
2.3 Rapp's December 1981 Potential Coefficients	11
3. Algorithm for Optimal Estimation of Potential Coefficients	14
3.1 Integration of Associated Legendre Functions	14
3.2 Generation of Normals	15
3.3 Optimal Quadrature Weights and Error Estimates	16
3.31 Reordering of the Normals	16
3.32 Reordering of the Right Hand Side Vectors	17
3.33 Solution of the Normals	19
3.4 Computation of Potential Coefficients	20
4. Potential Coefficient and Gravity Anomaly Data Sets	23
4.1 Anomaly Error Estimates	23
4.2 Data Sets A	24
4.3 Data Sets B	24
5. Comparison of Sets of Potential Coefficients	25
5.1 Initial Tests with Data Set A	26
5.2 Initial Tests with Data Set B	28
5.3 Test with Altered Anomaly Data Set	30
5.4 Improvement in Coefficients with Optimal Estimation	33
6. Optimal Estimation of Coefficients to Degree and Order 250	38
6.1 Magnitude Information by Degree	38
6.2 Error Estimates by Degree	43
6.3 Empirical Anomaly Degree Variances	50
7. Summary and Conclusions	55
7.1 Conclusions of Present Study	56
7.2 Recommendations for Further Investigations	57
References	59

## List of Figures

5.1	Location of Four $10^\circ \times 10^\circ$ Blocks where $1^\circ \times 1^\circ$ Anomalies were Set to Zero	31
5.2	Percentage Improvement per Degree due to Optimal Estimation of Coefficients	36
5.3	Improvement in Undulation and Anomaly per Degree due to Optimal Estimation of Coefficients	37
6.1	Coefficient Set B1: Undulation Magnitude per Degree	41
6.2	Coefficient Set B1: Anomaly Magnitude per Degree	42
6.3	Coefficient Percentage Error per Degree: Sets A, B1, B2	45
6.4	Cumulative Undulation Error: Sets A, B1, B2	48
6.5	Cumulative Anomaly Error: Sets A, B1, B2	49
6.6	Anomaly Degree Variances: Sets B1, B2, Kaula's Rule, A-priori Model	51
6.7	Comparison of Anomaly Degree Variances: Sets A and B2	53
6.8	Comparison of Anomaly Degree Variances: Sets A and B1	54

## List of Tables

3.1	CPU Time for Generating Normals for Estimating Coefficients to Degree NN	16
3.2	TAPE IO for Reordering Normals for Estimating Coefficients to Degree NN	17
3.3	Size of Array Needed for Reordering the RHS Vectors by Indexing for Estimating Coefficients to Degree NN	18
3.4	Algorithm for Optimal Estimation of Potential Coefficients from $1^{\circ} \times 1^{\circ}$ Global Anomaly Data	22
4.1	Average Anomaly Errors in $1^{\circ}$ Latitude Bands for Error Estimate A	23
5.1	Comparison of Potential Coefficient Sets A and B	25
5.2	Variation of Coefficients from De-smoothing Factors with Coefficients from Optimal Estimation	26
5.3	Variation of Optimally Estimated Coefficients with Variation in Anomaly Error Estimates	27
5.4	Agreements in Data Sets B Compared with Agreements in Data Sets A	29
5.5	Variation of Optimally Estimated Coefficients with Variation in Global Anomaly Data	32
5.6	Limits of Four $10^{\circ} \times 10^{\circ}$ Blocks where $1^{\circ} \times 1^{\circ}$ Anomalies were set to Zero	33
5.7	Improvement Due to Optimal Estimation of Coefficients	35
6.1	Variation of Optimally Estimated Coefficients to Degree 250 with Variation in Anomaly Error Estimate: Sets B1, B2	39
6.2	Undulation and Anomaly Magnitudes per Degree and Cumulatively: Sets B1, A	40
6.3	Coefficient Percentage Error Estimates per Degree by Optimal Estimation: Sets B1, B2	44
6.4	Undulation and Anomaly Error Estimates per Degree and Cumulatively: Sets B1, B2, A	47

## 1. INTRODUCTION

The earth's gravitational potential,  $V$ , at a point with geocentric coordinates  $(r, \phi', \lambda)$ , may be represented by a spherical harmonic expansion (Moritz, 1980a, Sec. 3):

$$V = V(r, \phi', \lambda) = \frac{GM}{r} \left[ 1 + \sum_{n=2}^{\infty} \sum_{m=0}^n \left(\frac{a}{r}\right)^n (\bar{C}_{nm} \cos m\lambda + \bar{S}_{nm} \sin m\lambda) \bar{P}_{nm}(\sin \phi') \right] \quad (1.1)$$

where  $GM$  is the gravitational constant times the earth's mass,  $a$  is the equatorial radius of the best-fitting earth ellipsoid;  $(\bar{C}_{nm}, \bar{S}_{nm})$  and  $\bar{P}_{nm}$  (function of  $\sin \phi'$ ,  $\phi'$  is geocentric latitude) are respectively the fully normalized potential, or harmonic, coefficients and associated Legendre functions of degree  $n$  and order  $m$ . If we subtract the potential coefficients corresponding to the earth's normal gravity field from  $(\bar{C}_{nm}, \bar{S}_{nm})$ , the residual potential coefficients  $(\bar{C}_{nm}^*, \bar{S}_{nm}^*)$  when substituted in (1.1) will yield the anomalous potential  $T$ .

As other quantities related to the earth's gravity field, e.g., gravity anomalies, geoid undulations, deflections of vertical, etc., are simply related to the anomalous potential  $T$ , a knowledge of the potential coefficients  $(\bar{C}_{nm}, \bar{S}_{nm})$  serves to describe the earth's gravity field. The computation of gravity related quantities from the potential coefficients may be termed as 'harmonic synthesis'. Several very efficient algorithms are now available for harmonic synthesis. A comparison of these algorithms is described by Tscherning et al. (1983). The inverse operation of computing potential coefficients from a global data set of gravity related quantity may be termed as 'harmonic analysis'. The algorithms for harmonic analysis will be described in Sections 2 and 3 of this study following the development by Colombo (1981).

The resolution of gravity related quantities computed by harmonic synthesis depends on the degree  $n$  up to which the potential coefficients are available. A dramatic improvement in the resolution of geoid undulations around Japan computed with potential coefficients up to degree  $n=180$ , when compared with  $n=36$ , may be seen in Rapp (1982, Figures 1 and 2). Another advantage of potential coefficient determination to a high degree, through harmonic analysis, is the use of residual quantities, referred to this high degree field, for evaluating integral formulas, e.g. computing geoid undulations from residual gravity anomalies. A much smaller residual data 'cap' would be adequate with the use of high degree field. For further discussion of the role of high degree field in solving geodetic problems, see Tscherning (1983).

A high degree potential coefficient field GEM10C to degree 180 was developed by Lerch et al. (1981) using global  $1^\circ \times 1^\circ$  mean geoid heights  $\bar{H}^*$ , residual to GEM10B (complete to degree 36), by implementing:

$$\begin{pmatrix} \bar{C}_{nm}^* \\ \bar{S}_{nm}^* \end{pmatrix} = \frac{1}{4\pi a} \iint_{\phi \lambda} \bar{H}^*(\phi, \lambda) \bar{P}_{nm}(\sin \phi) \begin{pmatrix} \cos m\lambda \\ \sin m\lambda \end{pmatrix} \cos \phi \, d\phi \, d\lambda \quad (1.2)$$

Rapp has developed several high degree fields, the current one to degree 180 is described in Rapp (1981). He utilized global  $1^\circ \times 1^\circ$  mean gravity anomalies which were first adjusted with a potential coefficients set to degree 36. The procedure will be discussed more fully in Section 2.3. In concept, the following relation was implemented:

$$\begin{pmatrix} \bar{C}_{nm}^* \\ \bar{S}_{nm}^* \end{pmatrix} = \frac{1}{4\pi\gamma(n-1)} \iint_{\sigma} \Delta g \bar{P}_{nm}(\sin \phi') \begin{pmatrix} \cos m\lambda \\ \sin m\lambda \end{pmatrix} d\sigma \quad (1.3)$$

where  $\Delta g$  is the gravity anomaly over a block size  $d\sigma$ ,  $\gamma$  is an average value of gravity over the globe, denoted by  $\sigma$ , and other notations are as in (1.1).

The main problems in implementing (1.2) or (1.3), or similar relations, are as follows. Firstly, the uncertainty in the gravity related quantity,  $\bar{H}^*$ ,  $\Delta g$ , etc., is not taken into account in computing the potential coefficients. These coefficients remain the same so long as the global data set, e.g. of gravity anomalies, is not changed, whether the uncertainty ascribed to the anomalies is 20 mgals, or 5 mgals, globally, or more realistically varies over the globe. Secondly, the error estimates of the potential coefficients are not obtained satisfactorily taking into account both the uncertainty or 'noise' of the gravity related quantity, and the finite block size, or 'sampling', over which this quantity is given as a mean value. Thirdly, in the practical implementation of (1.2), (1.3), etc., the integration is replaced by a summation, and the fact that we are using mean values instead of point values requires a choice of 'desmoothing' factors (see Rapp (1981), p. 4), depending on the degree of potential coefficients being computed. If a few desmoothing factors are chosen, separately for different degree bands, to span the entire spectrum, a sharp discontinuity may result at the boundary of degree bands. In fact, the current potential coefficients field by Rapp (1981) was developed to degree 300, but has been usually employed only up to degree 180 because of concern over such a discontinuity.

Colombo (1981) developed algorithms for 'optimal' estimation of potential coefficients which are free of the above problems. His tests were carried out with global set of  $5^\circ \times 5^\circ$  anomalies. He estimated CPU time of about two hours, on an Amdahl 470 V/6-II computer, for computing coefficients to degree 180 with a global set of  $1^\circ \times 1^\circ$  anomalies. With a faster 470 V/8 computer, and by slight modifications in the subroutines, we can now compute coefficients to degree 250 with  $1^\circ \times 1^\circ$  anomalies in about 60 minutes CPU time. This procedure will be described in Section 3.

The initial potential coefficients set used in this study is the one developed by Rapp (1981) to degree 180. We used this set to compute a global  $1^\circ \times 1^\circ$  anomaly data, which then served as a test data to generate different potential coefficient sets by optimal estimation procedure, assuming different error estimates for the anomaly data. Rapp (ibid.) had also generated an adjusted global  $1^\circ \times 1^\circ$  anomaly data set, adjusted with a potential coefficient set to degree 36. This was the second global anomaly data set used in the present study. The different potential coefficient sets, and the global anomaly data sets, are described in Section 4.

The differences between the various potential coefficient sets are examined in Section 5. This allows us to estimate the improvement by the optimal estimation procedure over the current (Rapp, 1981) harmonic analysis procedure in developing a high degree field. There are presently several areas in the world, which have geophysically predicted  $1^\circ \times 1^\circ$  anomalies. We therefore also examine in Section 3.3, the change in potential coefficients set if anomalies in some areas of the world are set to zero.

The potential coefficients developed to degree and order 250, and their error estimates, by optimal estimation procedure are discussed in Section 6. There is a very substantial improvement in these error estimates when compared with the error estimates of the current set of potential coefficients (Rapp, 1981). The error estimates of geoid undulations, and gravity anomalies, computed from the potential coefficients developed by optimal estimation, are also examined by degree, and cumulatively. Section 7 summarizes the findings of the present study. The choice of the highest degree 250, to which the coefficients will be estimated from  $1^\circ \times 1^\circ$  anomalies, was somewhat arbitrary. It was chosen from the dual consideration of keeping the computational effort manageable, and yet not lose the high degree information available in  $1^\circ \times 1^\circ$  anomalies. The reformulation of the computational algorithm in several steps is given later in Table 3.4. We will also find in Section 6, that at degree 250, the undulation magnitude per degree is about 1 cm, and the anomaly magnitude per degree is about 0.5 mgals.

ut on tape after rearranging as  $180 (=N_{\theta}(2.22))$  numbers,  $(NN+1)$  times, for 90 latitude bands. The requirement is to form them into  $(NN+1)R(m)$ ,  $m=0$  to  $NN$  matrices of  $180 \times 180$  numbers. The expansion of  $180 \times 90$  numbers into  $180 \times 180$  matrix, by exploiting the persymmetric nature of  $R(m)$  matrices, can be handled by proper indexing. However, reading 180 numbers as one logical record still requires  $90 \times (NN+1)$  records to be read to access the whole set to pick out elements of one  $R(m)$  matrix; and  $90 \times (NN+1)^2$  records to be read to form  $(NN+1) R(m)$  matrices, and additional TAPE IO for writing out the reordered  $R(m)$  matrices. Using the largest block size for reading and writing, the TAPE IO for different  $N$  are given in Table 3.2.

Table 3.2 TAPE IO for Reordering Normals for Estimating Coefficients to Degree  $NN$ .

NN	TAPE IO		
	Read	Write	Total
180	134, 121	724	134, 845
250	257, 777	1,004	258, 781
300	370, 832	1,204	372, 036

To avoid excessive TAPE IO costs, the coding was modified to put the sequential set of generated normals, after grouping  $180 \times (NN+1)$  numbers for  $k$  latitude bands as one record, on random disk storage. This not only removed the need to read the entire sequential set to form one  $R(m)$  matrix, but also allowed  $k$   $R(m)$  matrices to be assembled at a time, as any one record was read in from random storage. However, this required that an array of  $k \times (16,290) \times 8$  bytes should be available, where  $16,290 (= 180 \times 181/2)$  is the number of double precision elements in vector form of a  $180 \times 180$   $R(m)$  matrix.

With 2048 K bytes of virtual storage,  $k$  was chosen as 13. A proportionally larger value of  $k$  could be chosen if a larger region size is available. This step of reordering the normals may be termed as step 3A.

### 3.32 Reordering of the Right Hand Side Vectors

After the reordering of  $R(m)$  matrices,  $m=0$  to  $NN$ , we need to read in the right hand side vector  $k_{nm}$  in the following manner, for the solution of  $x_{nm}$  in (2.30). For  $k_{nm}$ , 180 elements for latitude bands  $i=0$  to 179, arranged by order  $n=0$  to  $NN$ , and degree  $n=m$  to  $NN$ ; where  $NN$  is the highest degree and order up to which coefficients are to be estimated, usually  $N < NN < N_{max}$ . From the 45,451  $k_{nm}^i$  values per latitude band,  $n=0$  to  $N_{max}$ ,  $m=0$  to  $n$ , available in step 1C, the values corresponding to  $m=0$  to  $NN$ ,  $n=m$  to  $NN$ , could be picked by suitable indexing in each latitude band, and multiplied by the factor in (3.4) to obtain corresponding  $k_{nm}^i$ . This would result in the elements of  $k_{nm}$  being assembled as  $(NN+1)(NN+2)/2$  elements,  $m=0$  to  $NN$ ,  $n=m$  to  $NN$ , for each latitude band  $i=0$  to 179. If we consider it as a general matrix stored in a vector form row by row,

$m=0$  to  $NN$ , for each row  $p$ . The procedure is repeated by reading in  $I_{nm}^i$  for  $i=1, 2, \dots, 89$  and implementing  $p=i$  to  $179-i$  for each  $i$ , thereby fully exploiting the equatorial symmetry of the data grid, which makes  $R(m)$  matrices persymmetrical, i.e., symmetrical with respect to both the main diagonal and the main antidiagonal.

For a given  $NN$ , the CPU time for generating  $r_m^{ip}$  varies almost linearly with the latitude band  $i$ , decreasing from high to low latitudes, except for slight reduction in the polar region for high  $NN$ . A modification was made to generate only a portion of the normals, i.e.  $r_m^{ip}$  for any one or more  $i$  (for all  $p=1$  to  $179-i$ ) for estimating the time to generate the entire normals for a given  $NN$ . Some CPU times on an Amdahl 470 V/8 computer are given in Table 3.1 for various  $NN$  for the case of  $1^\circ \times 1^\circ$  anomalies.

**Table 3.1** CPU Time for Generating Normals for Estimating Coefficients to Degree  $NN$ .

Latitude Band $i$	CPU Time in Seconds		
	$NN=12$	$NN=60$	$NN=250$
0	5.3	13.4	25.7
29	4.1	8.1	31.8
59	2.9	5.0	10.0
89	1.7	1.8	2.1
Total Time $i=0$ to $89$	$\approx 5.3$ min.	$\approx 10$ min.	$\approx 26$ min.

The generation of normals in this step 2 depends only on the data grid, e.g.  $\Delta\theta = \Delta\lambda = 1^\circ$ . As the error estimates of anomalies are introduced in later steps, the normals are not required to be regenerated for testing the effect of different anomaly error estimates.

### 3.3 Optimal Quadrature Weights and Error Estimates

The elements of  $R(m)$  matrices generated in step 2 in Section 3.2 first need to be arranged by the order  $m$ ,  $m=0$  to  $NN$ , in a vector form for the  $180 \times 180$  symmetric matrix, for all latitude bands  $i$  and  $p$ . Similarly, the elements  $I_{nm}^i$  in step 1C need to be arranged by the order  $m$  to assemble the vector  $k_{nm}$  in the form needed for implementing (2.30) to solve for  $x_{nm}$ , for all  $n$  for a given  $m$ . It is only at this stage that average variance  $\sigma_i^2$  of anomalies in (2.32) in different latitude bands has to be considered.

#### 3.31 Reordering of the Normals

$r_m^{ip}$  are generated in step 2 as  $(NN+1)$  numbers, for 180 latitude bands  $p$ , for 90 latitude bands  $i$  from pole to equator. The generated numbers are written

$$PI_{nm}^i, (i = 0 \text{ to } 89) = \begin{cases} + PI_{nm}^k, (k = 179-i); n - m = \text{even} \\ - PI_{nm}^k, (k = 179-i); n - m = \text{odd} \end{cases} \quad (3.3)$$

Finally, as the  $PI_{nm}^i$  are needed in the form of  $I_{nm}^i$  as in (2.24) for all further computations, a third tape was written for  $I_{nm}^i$  from north pole to south pole,  $i = 0$  to 179:

$$I_{nm}^i = \sqrt{\frac{c_n}{2n+1}} \cdot \frac{1}{\Delta_i} \cdot PI_{nm}^i = k_{nm}^i / \sqrt{\frac{c_n}{2n+1}} \quad (3.4)$$

These three steps of computing  $PI_{nm}^i$ ,  $i = 0$  to 89; extending  $PI_{nm}^i$  to  $i = 0$  to 179; and modifying these to  $I_{nm}^i$ ,  $i = 0$  to 179 are preliminary steps to the generation of normals. These three steps may be termed as 1A, 1B and 1C for convenience of reference. The anomaly degree variance model will be specified in Section 4.

### 3.2 Generation of Normals

The Fourier transforms,  $a_m^{ip}$ ,  $m = 0$  to  $n$ , of the covariances of anomaly blocks in two latitude bands  $i$  and  $p$  are obtained by (Colombo, 1981, p. 44, (2.63)):

$$a_m^{ip} = \left[ \sum_{n=m}^{N_{\max}} I_{nm}^i I_{nm}^p + \sum_{n=m}^{N_{\max}} I_{n,2N-m}^i I_{n,2N-m}^p \right] \cdot \begin{cases} \Delta\lambda^2 & \text{for } m=0 \\ \frac{2}{m^2} (1 - \cos m \Delta\lambda) & \text{for } m \neq 0 \end{cases} \quad (3.5)$$

where  $2N-m \leq N_{\max}$ . The second term in the square brackets take the aliasing of Fourier transform into account, with increasing  $m$ .  $N_{\max}$  was taken as 300 based on experiments by Colombo (1981, Sec. 4.2).

The element  $r_m^{ip}$ , corresponding to latitude bands  $i$  and  $p$ , of the matrix  $R(m)$ ,  $m = 0$  to  $NN$ , where  $NN$  is the highest degree up to which coefficients will be estimated ( $N < NN < N_{\max}$ ), are obtained by:

$$r_m^{ip} = a_m^{ip} \begin{cases} 2N, & \text{if } m=0 \\ N, & \text{if } m \neq 0 \end{cases} \quad (3.6)$$

The formation of  $R(m)$  matrix may be termed as the generation of normals in the frequency domain corresponding to the formation of the covariance matrix  $C_{zz}$  of the 64,800 anomaly blocks. This step of the algorithm takes a large CPU time. However, the CPU time is dependent on the highest degree up to which the coefficients are to be estimated, as the number of  $180 \times 180$   $R(m)$  matrices to be formed is  $NN+1$ .

The implementation of (3.5) starts by reading in the 45,451 values of  $I_{nm}^i$  in (3.4) in step 1C for  $i=0$ , and multiplying with the corresponding values of  $I_{nm}^p$  in (3.5) for  $p=0$  to 179 yielding  $NN+1$  numbers  $a_m^{op}$  (and  $r_m^{op}$  from (3.6)),

### 3. ALGORITHM FOR OPTIMAL ESTIMATION OF POTENTIAL COEFFICIENTS

The algorithm outlined in Section 2.2 was coded by Colombo (1981, Appx. B4) in subroutines NORMAL and ANALYS, and were tested by him up to the smallest anomaly block size of  $5^\circ \times 5^\circ$ , comprising of 2592 anomalies globally. In applying these subroutines to the case of 64,800  $1^\circ \times 1^\circ$  anomalies, it appeared advisable both for testing, and for actual computations, to separate out portions of NORMAL which could run sequentially, without repeating earlier stages and thus allowing greater flexibility in considering different anomaly uncertainties, and later different global anomaly data sets. Also, two major modifications were required because of very large TAPE/DISK IO's, or very large array size, needed with the existing coding for the case of  $1^\circ \times 1^\circ$  anomalies. The separate portions of implementing the algorithm and the modifications, are described below. The numerical values, and ranges, will refer to the case of  $1^\circ \times 1^\circ$  anomalies.

#### 3.1 Integration of Associated Legendre Functions

The integrals of associated Legendre functions,  $PI_{nm}^i$ ,

$$PI_{nm}^i = \int_{\theta_i}^{\theta_i + \Delta\theta} \bar{P}_{nm}(\cos \theta) \sin \theta d\theta \quad (3.1)$$

are needed repeatedly for implementing (2.20) and (2.21), e.g. in the formation of the elements of  $R(m)$  matrices and the array  $k_{nm}$  for computing the optimal quadrature weights  $x_{nm}$  in (2.30). The recursive relations for efficiently computing  $PI_{nm}^i$  were developed by Paul (1978). A subroutine supplied by him (private communication to R.H. Rapp) was used to generate PI on tape for:

$$0^\circ \leq \theta_i \leq 89^\circ, \Delta\theta = 1^\circ, n = 0 \text{ to } N_{\max}; m = 0 \text{ to } n; N_{\max} = 300 \quad (3.2)$$

These are nominal values of  $\Delta\theta$ , and  $\theta$  as the complement of geodetic latitude  $\phi$ . The actual integration limits in (3.1) were obtained by  $\theta = 90 - \phi'$ , by converting the nominal geodetic latitudes  $\phi$  to the corresponding geocentric latitudes  $\phi'$ . To avoid the numerical instability in computing the sectorial  $PI_{nm}^i$ , the direct series expansions were used for latitudes up to  $50^\circ$  from the pole for  $PI_{nm}^i$  instead of forward sectorial recurrence relations. This tape was already available for this study, but for any future studies with  $n$  exceeding 300, Gleason (1983) has suggested modifications to Paul's routines for employing backward and forward sectorial recursions depending on the condition number associated with the recursion (Gerstl, 1980).

The order of PI on tape was according to latitude bands from the north pole to the equator; and on each latitude band  $(N_{\max}+1)(N_{\max}+2)/2=45,451$   $PI_{nm}^i$  values were arranged by degree and order as in (3.2). As the  $PI_{nm}^i$  are required for all latitude bands from the north pole to the south pole for the elements in the right hand side of (2.30), a new tape was written by exploiting the symmetry of  $PI_{nm}^i$  with respect to the poles, and change of sign in the two hemispheres when  $(n-m)$  is odd:

We note from (2.40) that under the assumption of a constant global anomaly error, the propagated error estimate of all coefficients of different order are the same in each degree. This also appears to be the case in (2.41) for sampling error, but this is an artifact due to the fitting of the quartic expression in (2.41) to estimation errors  $\sigma_{en}$  per degree in (2.33) instead of estimation errors for each pair of coefficients  $C_{nm}^{\alpha}$  as discussed after (2.32).

Based on root mean square errors of 56,751 merged anomalies as  $\pm 10$  mgals, and  $\pm 30$  mgals for the balance 8049 anomalies, the constant global anomaly error  $m$  in (2.36) could be taken as  $\pm 15$  mgals. A larger value of  $\pm 20$  mgals was chosen to allow for possible anomaly errors in the several largely unsurveyed areas (Rapp, 1981, p. 15). This caused a slightly pessimistic coefficient error estimate in (2.40).

$$A = \frac{\sigma^2 \Delta\phi \Delta\lambda \mu_n}{[\gamma(n-1)]^2} \quad (2.36)$$

where  $\sigma$  is the standard error of a  $1^\circ \times 1^\circ$  anomaly, assumed to be the same for all 64,800 anomaly blocks; and  $\mu_n$  are the de-smoothing factors (2.7) in HARMIN.

$\underline{B}_\ell = \partial F / \partial \underline{L}_\ell^a$  are the partials in (2.34) and  $P_\ell$  is the weight matrix of anomalies, assumed to be diagonal,

$$[P_\ell] = \cos \phi' / \sigma^2 = \sin \theta / \sigma^2 \quad (2.37)$$

The corrections  $\underline{V}_\ell$  to the anomaly data set is obtained by:

$$\underline{V}_\ell = P_\ell^{-1} \underline{B}_\ell^T P_x \underline{V}_x \quad (2.38)$$

The simplification in the adjustment model results from  $\underline{B}_\ell P_\ell^{-1} \underline{B}_\ell^T$  matrix being diagonal (so that its inversion becomes trivially simple), which depends on the assumption (2.37) with the standard error  $\sigma$  of all anomalies being the same globally.

Elements of the covariance matrix  $E_{nx}$  of coefficient errors due to propagation of anomaly errors are given (Rapp, 1969, p. 112, (12)) by:

$$[E_{nx}] = \frac{A}{1 + [P_x]A} \quad (2.39)$$

$E_{nx}$  was considered as a diagonal matrix. The standard errors of 'adjusted SET1' coefficients to degree 36 (some additional coefficients to degree 48) were retained, while for higher degree and order coefficients  $P_x$  was null matrix and  $\mu_n$  in (2.7) was uniformly taken as  $1/4\pi$ . Then the diagonal elements of  $E_{nx}$  for coefficients, other than the 'adjusted SET1', were computed (Rapp, 1981, p. 29, (30)) by using (2.36) as:

$$[E_{nx}] = A = \frac{\sigma^2 \Delta\phi \Delta\lambda}{4\pi [\gamma(n-1)]^2} \quad (2.40)$$

The diagonal covariance matrix  $E_{ns}$  of coefficient errors due to sampling finite size of  $1^\circ \times 1^\circ$  anomaly blocks was based on empirical relation derived from a Montecarlo approach (Colombo, 1981, p. 78, (3.10)):

$$[E_{ns}] = \left[ \frac{\sigma_N}{100} \{ (-16.19570 \left(\frac{n}{N}\right) + 30.34506) \left(\frac{n}{N}\right) + 40.29588 \left(\frac{n}{N}\right)^2 \} \right]^2 \quad (2.41)$$

The Montecarlo experiments are described in Colombo (1981, Sec. 3.1) and the sampling error computations were performed as described in Section 2.2 of this study utilizing noise-free data.

### 2.3 Rapp's December 1981 Potential Coefficients

Rapp's current set of coefficients was developed (Rapp, 1981) to degree and order 300, but have been generally employed to degree and order 180. The procedure for computing these coefficients is reviewed here. In concept, the coefficients were computed as in Section 2.1, but the error estimates included sampling error based on Section 2.2.

First, a low degree potential coefficients set (complete to degree 36 with some additional coefficients to degree 48) was assembled by a weighted merging of most current sets, including resonance coefficients of orders 12 to 15 and 30. These merged coefficients were called SET1, and were also assigned error estimates. Similarly, a global set of 64,800 1°x1° mean gravity anomalies was assembled by merging most current terrestrial anomaly data with anomalies determined from adjusted Seasat altimeter data. The number of merged anomalies was 56,751 with root mean square of standard errors of anomalies being ±10 mgals. The remaining 8049 anomalies, to complete the global set, were assigned values implied by SET1 coefficients, and assigned standard error of 30 mgals.

Next, a simplified adjustment was made, whose procedure is outlined below, of SET1 coefficients and 64,800 1°x1° anomalies. The result of the adjustment may be called 'adjusted SET1' to degree 36 (some additional coefficients to degree 48), and 64,800 'adjusted anomalies'. The 'adjusted anomalies' were used to compute potential coefficients to degree 300 using subroutine HARMIN, which implements (2.5) with de-smoothing factors (2.7). The 'adjusted anomalies' and the coefficients (using HARMIN) up to degree 180 will be termed test data set B in Section 4.2. Because of the simplified adjustment procedure, the low degree coefficients in data set B did not fully agree with the 'adjusted SET1' coefficients, though the difference was small as discussed later in Section 5. A merged set of coefficients was then formed using 'adjusted SET1' where available (complete to degree 36, with some additional coefficients to degree 48), and the remaining high degree coefficients as developed from 'adjusted anomalies' using HARMIN. This merged set up to degree 180 are Rapp's current (December 1981) potential coefficients, and will be part of test data set A in Section 4.2.

The simplified adjustment of combining SET1 with global anomaly data is based on the model:

$$F = F(\underline{L}_x^a, \underline{L}_g^a) = 0 \quad (2.34)$$

where  $\underline{L}_x^a$  are the adjusted SET1 coefficients, while  $\underline{L}_g^a$  are the adjusted anomalies. Denoting one element as  $[\cdot]$ , an element  $[V_x]$  of the correction vector  $\underline{V}_x$  to SET1 coefficients is given by:

$$[V_x] = -[w]/(1 + A[P_x]) \quad (2.35)$$

where  $w$  is the misclosure vector between the SET1 coefficients and the computed coefficients from the anomalies using HARMIN,  $P_x$  is the weight matrix (assumed to be diagonal) for the SET1 coefficients, and  $A$  is one of the elements of the diagonal matrix  $\underline{B}_x P_x^{-1} \underline{B}_x^T$ , given by (Rapp, 1981, p. 6, (23)):

(2.31) allows harmonic analysis through a quadrature formula, and  $\underline{x}_{nm}$  may be called the optimal quadrature weights. The optimal quadrature weights are derived on the basis of minimizing the sum of both error quadratic terms due to finite size of anomaly blocks, and the anomaly uncertainties. And (2.31) retains the efficiency in computation of the coefficients inherent in the structure of  $(C_{zz}+D)$  discussed before (2.24). This however requires (Colombo, 1981, Sec. 2.9) a slight modification in the structure of noise matrix  $D$ . The modification is that the variances for all anomalies in a latitude band be equated to the average value for that band, i.e.

$$\sigma_i^2 = \frac{1}{2N} \sum_{j=0}^{2N-1} \sigma_{ij}^2 \quad (2.32)$$

This modification causes a change in estimates for propagated error ( $e_n$  in (2.15)) for non-zonal coefficients. But the sum of variance of a pair of non-zonal coefficients  $\bar{C}_{nm}^\alpha$ , i.e.  $(\bar{C}_{nm}, \bar{S}_{nm})$ , is unaltered. The estimated variance of each of the coefficients, in a pair, is then arbitrarily made equal. This is a minor modification to retain the computational efficiency of not having to directly invert the  $(C_{zz}+D)$  matrix of a large size.

There is no change in error estimates of the zonal coefficients. There is also no change in the error variance per degree,  $\sigma_{\epsilon n}^2$ , or the error variance per average coefficient per degree,  $\bar{\sigma}_{\epsilon n}^2$ :

$$\sigma_{\epsilon n}^2 = \sum_{m=0}^n \sum_{\alpha=0}^1 \sigma_{nm\alpha}^2 = \sum_{m=0}^n (\sigma_{cnm}^2 + \sigma_{snm}^2) \quad ; \quad \bar{\sigma}_{\epsilon n}^2 = \frac{\sigma_{\epsilon n}^2}{2n+1} \quad (2.33)$$

The implementation of (2.23) to (2.29), leading to the computation of optimal quadrature weights in (2.30) is done by subroutine NORMAL. The error estimates for the coefficients, obtained in concept through (2.21), are also computed by NORMAL, including (2.33), under the condition (2.32). The optimal quadrature weights,  $\underline{x}_{nm}$ , computed by NORMAL, are used in subroutine ANALYS with the global anomaly data for the harmonic analysis of coefficients in (2.31). The coding of NORMAL and ANALYS is documented in Colombo (1981, Appx. B4). Some changes made in these subroutines will be discussed in Section 3.

One may notice the similarity of (2.5) and (2.6), the quadrature formula with de-smoothing factors  $\mu_n$ , and (2.31) read with (2.28), (2.26), (2.30), i.e. the quadrature formula with optimal quadrature weights  $\underline{x}_{nm}$ . As already mentioned,  $\underline{x}_{nm}$  are dependent on the anomaly uncertainties through (2.30), while  $\mu_n$  computed through (2.7) and (2.8) do not take into account the anomaly uncertainties. Hence, the coefficients computed in Section 2.1 will remain the same whether the global anomaly data has standard error, as an example, of 5 mgals, or 20 mgals, or more realistically varies over the globe. However, the estimated coefficients in Section 2.2 would realistically reflect the uncertainties in the estimate of anomalies, subject to the averaging of variance in a latitude band in (2.32). Section 2.2 coefficients are also optimal in the sense of minimizing  $E_T$  in (2.16), and satisfactorily accounting for both  $E_S$  and  $E_N$ , and also do not show any discontinuities which are caused in Section 2.1 coefficients due to (2.7).

$$\underline{c}_{nm\alpha, z} = \frac{c_n}{2n+1} \left[ \dots \frac{1}{\Delta\lambda} \int_{\theta_i}^{\theta_i+\Delta\theta} \overline{P}_{nm}(\cos \theta) \sin \theta \, d\theta \int_{\lambda_j}^{\lambda_j+\Delta\lambda} \underline{c}_m^\alpha \, d\lambda \dots \right]^T, \quad (2.25)$$

i=0 to (N<sub>θ</sub>-1)

$$= \left[ \dots k_{nm}^i \int_{\lambda_j}^{\lambda_j+\Delta\lambda} \underline{c}_m^\alpha \, d\lambda \dots \right]^T \quad (2.26)$$

where  $\underline{c}_m^\alpha = \left[ \dots \begin{pmatrix} \cos \\ \sin \end{pmatrix} m j \Delta\lambda \dots \right]^T, \quad j=0 \text{ to } (N_\lambda-1)$  (2.27)

and  $\int_{\lambda_j}^{\lambda_j+\Delta\lambda} \begin{pmatrix} \cos \\ \sin \end{pmatrix} m \lambda \, d\lambda = \left[ \begin{pmatrix} A(m) \\ -B(m) \end{pmatrix} \cos m j \Delta\lambda + \begin{pmatrix} B(m) \\ A(m) \end{pmatrix} \sin m j \Delta\lambda \right]$  (2.28)

where  $A(m) = \begin{cases} \Delta\lambda \\ (\sin m \Delta\lambda)/m \end{cases}, B(m) = \begin{cases} 0 \\ (\cos m \Delta\lambda - 1)/m \end{cases}, \quad \text{if } m=0 \\ \text{if } m \neq 0$  (2.29)

If we collect  $k_{nm}^i$  for all latitude bands  $i=0$  to  $(N_\theta-1)$  to define  $\underline{k}_{nm}$  and similarly collect  $x_{nm}^i$  for all latitude bands to define  $\underline{x}_{nm}$ , see below, i.e.,

$$\underline{k}_{nm} = [k_{nm}^0 \dots k_{nm}^i \dots k_{nm}^{N_\theta-1}]^T$$

$$\underline{x}_{nm} = [x_{nm}^0 \dots x_{nm}^i \dots x_{nm}^{N_\theta-1}]^T$$

where  $\underline{x}_{nm} = (R(m)+W)^{-1} \underline{k}_{nm}$ , (2.30)

W being the diagonal matrix consisting of average anomaly variance in each latitude band (see (2.32) below); then Colombo (1981, p. 43, (2.61)) shows that elements of vector  $\hat{c}$  in (2.20) may be computed by:

$$\hat{c}_{nm}^\alpha = \frac{1}{\gamma(n-1)} \sum_{i=0}^{N-1} x_{nm}^i \sum_{j=0}^{2N-1} \left[ \begin{pmatrix} A(m) \\ -B(m) \end{pmatrix} \cos m j \Delta\lambda + \begin{pmatrix} B(m) \\ A(m) \end{pmatrix} \sin m j \Delta\lambda \right] \overline{\Delta g}_{ij} \quad (2.31)$$

where we have substituted N for N<sub>θ</sub> and 2N for N<sub>λ</sub> in view of (2.4) and (2.22).

The formation and inversion of  $(C_{zz} + D)$  for 64,800  $1^\circ \times 1^\circ$  anomalies in (2.20) and (2.21) would be a formidable task. But Colombo (1979) has shown that under general conditions fulfilled by equi-angular grids, each covariance matrix between  $1^\circ \times 1^\circ$  anomaly blocks in two latitude bands has Toeplitz circulant structure (Colombo, 1981, Sec. 2.10). The main requirement of the same constant value of  $\Delta\lambda$  in each of the  $N$  latitude bands in (2.4):

$$\Delta\lambda = \lambda_{j+1} - \lambda_j; j = 0 \text{ to } 359 \text{ for all } \theta_i; i = 0 \text{ to } 179$$

$$\Delta\theta = \theta_{i+1} - \theta_i; \Delta\theta = \Delta\lambda = 1^\circ; N_\theta = \frac{\pi}{\Delta\theta} = 180; N_\lambda = \frac{2\pi}{\Delta\lambda} = 360 \quad (2.22)$$

is naturally fulfilled for equi-angular grid (the numbers correspond to  $1^\circ \times 1^\circ$  grid).

The structure of  $(C_{zz} + D)$  makes it possible that its inversion can be equivalently substituted (Colombo, 1981, p. 42, (2.54)) by the much simpler inversion of  $N_\theta \times N_\theta$  matrices  $R(m)$ ,  $m=0$  to  $\frac{1}{2}N_\lambda$ , if we wish to solve only for coefficients up to the Nyquist frequency given by  $N_\theta = \frac{1}{2}N_\lambda$ . However, if we were to solve for coefficients up to degree  $NN > N_\theta$ , it will require the formation of:

$$N_\theta \times N_\theta \text{ matrices } R(m), m=0 \text{ to } NN \quad (2.23)$$

However, their inversion is still a relatively simple problem as their size is  $N_\theta \times N_\theta$ . Also, the elements of  $R(m)$ , which are related to the discrete Fourier transform of covariances of anomaly blocks in a pair of latitude bands, can be obtained directly without actually computing the anomaly covariances. This requires repeated manipulation (Colombo, 1981, Sec. 2.11) of integrals  $I_{nt}^i$  of associated Legendre functions in the form:

$$I_{nt}^i = \sqrt{\frac{c_n}{2n+1}} \cdot \frac{1}{\Delta_i} \int_{\theta_i}^{\theta_i + \Delta\theta} P_{nt}^i(\cos \theta) \sin \theta \, d\theta = k_{nt}^i / \sqrt{\frac{c_n}{2n+1}} \quad (2.24)$$

where subscript  $t$  is related to the order  $m$ ,  $k_{nt}^i$  is defined in (2.25) below, other notations are as in (2.1), (2.4), (2.6); and  $c_n$  are the anomaly degree variances. The computation of integrals in (2.24) will be discussed in Section 3.1; the computation of the elements of matrices  $R(m)$  will be discussed in Section 3.2, and the anomaly degree variance model will be specified in Section 4.

The components  $\underline{c}_{nm\alpha}^T$ ,  $\underline{z}$  of the cross-covariance matrix  $C_{Cz}$  in (2.20), (2.21) are computed, for degree  $n$  and order  $m$ , by:

where  $\underline{e}_n$  represents the propagated noise, while  $\underline{e}_s$  may be interpreted as the sampling error.  $\underline{e}_s$  would tend to zero if perfect data (without any error or noise) was employed in (2.13), and the number of data points tended to infinity; or in other words, the mean anomaly block size tend to zero. We assume that the errors  $\underline{e}_s$  and  $\underline{e}_n$  arise due to completely independent causes.

The total covariance matrix  $E_T$  of the potential coefficient errors, may then be written as the sum of covariance matrices of errors  $E_s$  due to sampling and  $E_n$  due to data noise:

$$\begin{aligned} E_T &= E_s + E_n = M \{ \underline{e}_s \underline{e}_s^T \} + M \{ \underline{e}_n \underline{e}_n^T \} \\ &= M \{ (\underline{c} - F\underline{z})(\underline{c} - F\underline{z})^T \} + M \{ F\underline{n} \underline{n}^T F^T \} \end{aligned} \quad (2.16)$$

where  $M \{ \}$  is the averaging operator.

(2.16) is easily simplified to:

$$E_T = C - 2C_{CZ}F^T + F(C_{ZZ} + D)F^T \quad (2.17)$$

where

$$C = M \{ \underline{c} \underline{c}^T \}, \quad C_{CZ} = M \{ \underline{c} \underline{z}^T \}, \quad C_{ZZ} = M \{ \underline{z} \underline{z}^T \} \quad (2.18)$$

$$D = M \{ \underline{n} \underline{n}^T \}$$

are the covariance matrix of the coefficients, cross covariance matrix of coefficients and mean anomalies, covariance matrix of mean anomalies, and covariance matrix of mean anomaly errors, respectively.

An optimal value of estimator operator  $F$  in (2.13) may now be obtained, which will minimize the sum of square of total errors for all coefficients, i.e. the trace of  $E_T$ , by setting  $\partial \text{tr}[E_T]/\partial F$  to zero. This leads (Colombo, 1981, Sec. 2.8) to the well-known relations in least squares collocation:

$$F = C_{CZ}(C_{ZZ} + D)^{-1} \quad (2.19)$$

and by inserting (2.19) in (2.13) and (2.17), we get:

$$\hat{\underline{c}} = C_{CZ}(C_{ZZ} + D)^{-1}(\underline{z} + \underline{n}) = C_{CZ}(C_{ZZ} + D)^{-1}\underline{\Delta g} \quad (2.20)$$

$$E_T = C - C_{CZ}(C_{ZZ} + D)^{-1}C_{CZ}^T \quad (2.21)$$

For the case of harmonic synthesis, we may write for the point and mean anomalies:

$$\Delta g(\theta_i, \lambda_j) = \gamma \sum_{n=2}^{\infty} (n-1) \sum_{m=0}^n \sum_{\alpha=0}^1 \bar{C}_{nm}^{\alpha} \bar{Y}_{nm}^{\alpha}(\theta_i, \lambda_j) \quad (2.9)$$

$$\overline{\Delta g}_{ij} = \frac{\gamma}{\Delta_{ij}} \sum_{n=2}^{\infty} (n-1) \sum_{m=0}^n \sum_{\alpha=0}^1 \bar{C}_{nm}^{\alpha} \int_{\sigma_{ij}} \bar{Y}_{nm}^{\alpha}(\theta, \lambda) d\sigma \quad (2.10)$$

However, as the potential coefficients are available only up to degree  $n \leq N_{\max}$ , in the practical implementation of (2.10) the estimate  $\overline{\Delta g}_{ij}$  is affected by the truncation error at  $N_{\max}$  (and similarly for (2.9)):

$$\hat{\overline{\Delta g}}_{ij} = \frac{\gamma}{\Delta_{ij}} \sum_{n=2}^{N_{\max}} (n-1) \sum_{m=0}^n \sum_{\alpha=0}^1 \bar{C}_{nm}^{\alpha} \int_{\sigma_{ij}} \bar{Y}_{nm}^{\alpha}(\theta, \lambda) d\sigma \quad (2.11)$$

Subroutine HARMIN implements the harmonic analysis (2.5) using the de-smoothing factors in (2.7). Subroutine SSYNTH implements the harmonic synthesis (2.11). The coding of these subroutines is documented in Colombo (1981, Appx. B2, B3).

## 2.2 Quadrature Formulas with Optimal Weights

If we consider the global mean gravity anomaly vector  $\overline{\Delta g}$  to comprise two parts, the signal  $\underline{z}$  and the noise  $\underline{n}$ , i.e.,

$$\overline{\Delta g} = \underline{z} + \underline{n} \quad (2.12)$$

and denoting the potential coefficients vector  $[\bar{C}_{nm}^{\alpha}]$ ,  $m=0$  to  $n$ ,  $n=0$  to  $N_{\max}$  by  $\underline{c}$ , which is estimated from the anomaly data through a system of linear equations denoted by the matrix operator  $F$ , we may write:

$$\hat{\underline{c}} = F(\underline{z} + \underline{n}) \quad (2.13)$$

An optimal value of the estimator operator  $F$  will be derived later in (2.19).

The estimation error vector  $\underline{e}$  may then also be broken into two parts  $\underline{e}_s$  and  $\underline{e}_n$ :

$$\underline{e} = \underline{c} - \hat{\underline{c}} = \underline{c} - F(\underline{z} + \underline{n}) = (\underline{c} - F\underline{z}) - (F\underline{n}) \quad (2.14)$$

$$\underline{e}_s = \underline{c} - F\underline{z} ; \quad \underline{e}_n = F\underline{n} \quad (2.15)$$

(2.3) may be termed as the 'point value-type' quadrature formula as it assumes that the value of  $\Delta g$  and  $\bar{V}_{nm}^\alpha$  at  $\theta_j, \lambda_j$  (or perhaps at the center of the block  $\theta_j + \frac{\Delta\theta}{2}, \lambda_j + \frac{\Delta\lambda}{2}$ ) is constant over the whole block  $\Delta_{ij}$ . We may easily integrate  $\bar{V}_{nm}^\alpha$  over the block, but by keeping  $\bar{\Delta g}$  outside the integral in (2.5) below implies a very 'smooth' gravity anomaly signal over the block equal to the mean value. This can be remedied by multiplying by a 'de-smoothing' factor,  $\mu_n$  (Colombo, 1981, p. 33), so that we have a 'mean value-type' quadrature formula:

$$\hat{C}_{nm}^\alpha = \frac{\mu_n}{\gamma(n-1)} \sum_{i=0}^{N-1} \sum_{j=0}^{2N-1} \bar{\Delta g}_{ij} \int_{\sigma_{ij}} \bar{V}_{nm}^\alpha(\theta, \lambda) d\sigma, \quad (2.5)$$

where

$$\int_{\sigma_{ij}} \bar{V}_{nm}^\alpha(\theta, \lambda) d\sigma = \int_{\theta_i}^{\theta_i + \Delta\theta} \bar{P}_{nm}(\cos \theta) \sin \theta d\theta \int_{\lambda_j}^{\lambda_j + \Delta\lambda} \begin{cases} \cos \\ \sin \end{cases} m\lambda d\lambda, \quad \begin{matrix} \alpha=0 \\ \alpha=1 \end{matrix} \quad (2.6)$$

The evaluation of the integral of associated Legendre functions in (2.6) will be discussed in Section 3.1. The de-smoothing factor  $\mu_n$  may be related to the Pellinen/Meissl smoothing, or averaging, operator  $\beta_n$  (Rapp, 1977). By numerical tests for blocks of  $5^\circ \times 5^\circ$  and larger, Colombo (1981, p. 76, (3.9)) found a simple nearly optimal relationship:

$$\mu_n = \frac{1}{4\pi\eta_n}, \quad \eta_n = \begin{cases} \beta_n^2, & 0 \leq n \leq N/3 \\ \beta_n, & N/3 < n \leq N \\ 1, & n > N \end{cases} \quad (2.7)$$

The use of various de-smoothing factors in (2.7) may cause a sharp discontinuity in the potential coefficients at degree  $N/3$ , and at degree  $N$ , as was noticed by Rapp (1981, p. 24). Further,  $\mu_n$  takes into account only the block size, as  $\beta_n$  is given by:

$$\beta_n = \cot \frac{\psi_0}{2} \frac{P_{n1}(\cos \psi_0)}{n(n+1)} \quad (2.8)$$

where  $\psi_0$  is the radius of a circular cap having the same area  $\sigma_{ij}$  of the block. But  $\mu_n$  does not take into account the error estimate of  $\bar{\Delta g}$  employed in (2.5). Hence, Colombo (1981) also considered the rigorous determination of 'optimal quadrature weights',  $\chi_{nm}^i$ , based on the minimization of the sum of two quadratic terms, one due to 'sampling error', and the other due to 'data noise'. This is discussed in Section 2.2.

## 2. HARMONIC ANALYSIS AND SYNTHESIS

We will henceforward consider  $1^\circ \times 1^\circ$  mean anomalies, referred to the Geodetic Reference System 1980 (Moritz, 1980b), as the specific gravity related quantity, as in (1.3). We will also adopt a more compact notation:

$$\bar{C}_{nm}^\alpha \equiv \begin{cases} \bar{C}_{nm}, & \alpha=0 \\ \bar{S}_{nm}, & \alpha=1 \end{cases} \quad (2.1a)$$

$$\bar{Y}_{nm}^\alpha(\theta, \lambda) \equiv \begin{cases} \bar{P}_{nm}(\cos \theta) \cos m\lambda, & \alpha=0 \\ \bar{P}_{nm}(\cos \theta) \sin m\lambda, & \alpha=1 \end{cases} \quad (2.1b)$$

where we have expressed the functions in (2.1b) in terms of co-latitude  $\theta$ , instead of geocentric latitude  $\phi'$ . We will henceforward assume as in (2.1a) that the potential coefficients  $\bar{C}_{nm}^\alpha$ , i.e.  $\{\bar{C}_{nm}, \bar{S}_{nm}\}$ , are the residual potential coefficients to the ellipsoidal field of GRS 80, and we will dispense with the notation of superscript asterisk to denote such residual quantities.

### 2.1 Quadrature Formulas with De-smoothing Factors

We may then rewrite (1.3) for harmonic analysis as follows:

$$\bar{C}_{nm}^\alpha = \frac{1}{4\pi\gamma(n-1)} \iint_{\sigma} \Delta g(\theta, \lambda) \bar{Y}_{nm}^\alpha(\theta, \lambda) d\sigma \quad (2.2)$$

To implement (2.2), we first replace the integral by summation over the anomaly blocks; and the estimate  $\hat{C}_{nm}^\alpha$  is now affected by the 'sampling error' because of the finite area,  $\Delta_{ij}$ , of the actual anomaly blocks, in the numerical quadrature formula:

$$\hat{C}_{nm}^\alpha = \frac{1}{4\pi\gamma(n-1)} \sum_{i=0}^{N-1} \sum_{j=0}^{2N-1} \Delta g(\theta_i, \lambda_j) \bar{Y}_{nm}^\alpha(\theta_i, \lambda_j) \Delta_{ij} \quad (2.3)$$

$$\Delta_{ij} = \Delta\lambda (\cos\theta_i - \cos(\theta_i + \Delta\theta)) = \Delta_i \text{ for all } j \text{ in any latitude band } i,$$

$$\Delta\lambda = \lambda_{j+i} - \lambda_j, \Delta\theta = \theta_{i+1} - \theta_i; \Delta\theta = \Delta\lambda = 1^\circ, N = \frac{\pi}{\Delta\theta} = 180 \quad (2.4)$$

where the numerical values of  $\Delta\theta$ ,  $\Delta\lambda$ ,  $N$  have been shown for  $1^\circ \times 1^\circ$  equi-angular blocks.

the correct order of  $k_{nm}$  required is the vector form of the matrix stored column by column. This would then allow the right hand side vectors to be read in successively as 180 numbers at a time for a given  $R(m)$  matrix ( $m=0$  to  $NN$ ), for solving 180 numbers of  $x_{nm}$  for the given  $m$ , for degrees  $n=m$  to  $NN$ .

This reordering of the right hand side vectors, analogous to the transpose of a matrix, is a trivial problem if the whole matrix could be indexed as one array. In fact, by the exploitation of symmetries in (3.3), it would be sufficient to reorder the right hand side vectors, obtained from  $I_{nm}^1$  in the manner indicated above for  $i=0$  to 89; and after reordering the 90 elements of each right hand side vector, extend it to 180 elements using (3.3). However, the array dimension required for reordering the right hand side by indexing is not possible for the case of  $1^\circ \times 1^\circ$  anomalies, as is apparent from Table 3.3.

**Table 3.3** Size of Array Needed for Reordering the Right Hand Side Vectors by Indexing for Estimating Coefficients to Degree  $NN$ .

Degree NN	# Elements in $k_{nm}$		Array Dimension (Double Precision) in Mega Bytes
	$(NN+1)(NN+2)/2$ each $i$	Total $i=0$ to 89	
180	16,471	1,482,390	11.86 MB
250	31,626	2,846,340	22.77 MB
300	45,451	4,090,590	32.72 MB

The problem of reordering was solved by using IBM utility SORT. After the elements of  $k_{nm}$  were correctly ordered in a latitude band  $i$ ,  $m=0$  to  $NN$ ,  $n=m$  to  $NN$ , they were tagged with a number  $k$ ,

$$k = j * 100 + (i+1); \quad j=1 \text{ to } NLL, \quad i=0 \text{ to } 89; \quad NLL = (NN+1)(NN+2)/2 \quad (3.7)$$

and written on tape. After the tagged numbers were sorted in ascending sequence by SORT, they were in the order needed in (2.30). The number tag was stripped, and the right hand side vector  $k_{nm}$  written out on another tape. This step of reordering  $k_{nm}$  may be termed as step 3B. The CPU time by the SORT routine for sorting 2.8 million elements of  $k_{nm}$  for  $NN=250$  on an Amdahl 470 V/8 computer was 2 min. 58 sec., while the initial tagging of numbers took 3 min. 2 sec., and the writing out of sorted numbers took 2 min. 33 sec.

It may be noted that steps 2, 3A and 3B do not depend on the  $1^\circ \times 1^\circ$  anomaly error estimates, or the anomalies, but depend on the degree  $NN$  up to which coefficients are to be estimated. The testing of the effect of different anomaly errors, or different anomaly data sets may therefore be tried for low values of  $NN$  like 12, or 60, or 180, before developing coefficients to the highest degree.

### 3.33 Solution of the Normals

The solution of the normals in (2.30) proceeds by reading in the reformatted normals  $R(m)$  in step 3A, which is the vector form of the upper diagonal of symmetric  $180 \times 180$  matrix. The average variance  $\sigma_i^2$  in (2.32) of anomalies in each latitude band  $i$ ,  $i=0$  to 179, is added to the diagonal elements of  $R(m)$ , yielding the matrix  $(R(m)+W)$  in (2.30). This is done for each  $R(m)$  matrix, one at a time, for  $m=0$  to  $NN$ .

After inversion of  $(R(m)+W)$ , 90 numbers of the reordered right hand side vectors in step 3B are read in, expanded to 180 numbers by utilizing the symmetries in (3.3), and the optimal quadrature weights  $x_{nm}$  are solved for 180 numbers at a time,  $x_{nm}^i$ ,  $i=0$  to 179. The solution proceeds for each  $m=0$  to  $NN$ ,  $n=m$  to  $NN$ , requiring  $(NN+1)$  matrix inversions, and  $(NN+1)(NN+2)/2$  solutions. The CPU time for this step increases sharply for large  $NN$ . An Amdahl 470 V/8 computer took about 34 minutes CPU time for this step at  $NN=250$ .

The total error variance estimates in (2.21) are computed by:

$$\sigma_{c_{nm}}^2 = \sigma_{s_{nm}}^2 = \frac{1}{\gamma^2(n-1)^2} \left[ \frac{c_n}{2n+1} - \begin{cases} \Delta\lambda^2 & \text{if } m=0 \\ \frac{1-\cos m\Delta\lambda}{m^2} & \text{if } m \neq 0 \end{cases} \right] \cdot 2N \cdot \sum_{i=0}^{N-1} k_{nm}^i x_{nm}^i \quad (3.8)$$

which follows from the similarity of terms in (2.20) and (2.21); and the expressions (2.31) and (2.26) using  $x_{nm}^i$  and  $k_{nm}^i$ . The variances were earlier computed only for a pair of coefficients, unless  $m=0$ , as discussed below (2.32). A modification was made to compute the standard error of each coefficient; and the factor of  $\frac{1}{2}$  for  $m \neq 0$ , for making the variance for each coefficient in a pair equal, i.e.  $\sigma_{c_{nm}}^2 = \sigma_{s_{nm}}^2$ , has been incorporated in (3.8)

The error variance  $[E_n]_{c_{nm}} = [E_n]_{s_{nm}}$ , for each coefficient due to propagated noise is computed similarly to (3.8) by:

$$[E_n]_{c_{nm}} = [E_n]_{s_{nm}} = \frac{1}{\gamma^2(n-1)^2} \left[ \frac{c_n}{2n+1} - \begin{cases} \Delta\lambda^2 & \text{if } m=0 \\ \frac{1-\cos m\Delta\lambda}{m^2} & \text{if } m \neq 0 \end{cases} \right] \cdot 2N \cdot \sum_{i=0}^{N-1} x_{nm}^i \sigma_i^2 \quad (3.9)$$

And, the error variances due to sampling finite size of  $1^\circ \times 1^\circ$  anomaly blocks is computed by:

$$[E_s]_{c_{nm}} = [E_s]_{s_{nm}} = \sigma_{c_{nm}}^2 - [E_n]_{c_{nm}} = \sigma_{s_{nm}}^2 - [E_n]_{s_{nm}} \quad (3.10)$$

The program sums up the variances per degree due to sampling, propagated noise, and total. Modification was made to also compute other statistics for corresponding standard errors per degree, percentage sampling and noise errors of the total error, and also percentages of the errors per potential coefficient variation,  $\sigma_n$ , per degree:

$$\sigma_n = \sqrt{c_n} / (\gamma(n-1)) \quad (3.11)$$

This step of solving the normals for computing the optimal quadrature weights and the error estimates for the coefficients, based on average anomaly variances in different latitude bands, may be termed as step 3C.

### 3.4 Computation of Potential Coefficients

The computations of potential coefficients in (2.31), from the optimal quadrature weights  $\underline{x}_{nm}$  obtained in step 3C, is done by the harmonic analysis of global anomaly data by subroutine ANALYS. The computations are shortened by recognizing that the symmetries in (3.3) also apply to  $\underline{x}_{nm}$ . Hence, (2.31) is transformed to:

$$\hat{c}_{nm}^{\alpha} = \frac{1}{\gamma(n-1)} \sum_{i=0}^{\frac{1}{2}N-1} \left( x_{nm}^i \left[ \sum_{j=0}^{2N-1} \begin{pmatrix} A(m) \\ -B(m) \end{pmatrix} \cos mj \Delta \lambda + \begin{pmatrix} B(m) \\ A(m) \end{pmatrix} \sin mj \Delta \lambda \right] \overline{\Delta g}(\theta_i, \lambda_j) \right) +$$

$$(-1)^{n-m} x_{nm}^i \left[ \sum_{j=0}^{2N-1} \begin{pmatrix} A(m) \\ -B(m) \end{pmatrix} \cos mj \Delta \lambda + \begin{pmatrix} B(m) \\ A(m) \end{pmatrix} \sin mj \Delta \lambda \right] \overline{\Delta g}(\theta_{N-1-i}, \lambda_j) \quad (3.12)$$

The implementation of (3.12) is further speeded up by computing  $a_m^i, b_m^i, a_m^{N-1-i}, b_m^{N-1-i}$  as the Fourier transform along latitude bands  $i$  and  $N-1-i$  of the values of  $\overline{\Delta g}(\theta, \lambda)$ , i.e.

$$\begin{pmatrix} a_m^i \\ b_m^i \end{pmatrix} = \sum_{j=0}^{2N-1} \begin{pmatrix} \cos \\ \sin \end{pmatrix} mj \Delta \lambda \overline{\Delta g}(\theta_i, \lambda_j) \quad (3.13)$$

$$\begin{pmatrix} a_m^{N-1-i} \\ b_m^{N-1-i} \end{pmatrix} = \sum_{j=0}^{2N-1} \begin{pmatrix} \cos \\ \sin \end{pmatrix} mj \Delta \lambda \overline{\Delta g}(\theta_{N-1-i}, \lambda_j)$$

A modification was made to ANALYS to compute several sets of coefficients in the same run, either combining several sets of optimal quadrature weights associated with different anomaly error estimates with one global anomaly data set, or by utilizing different anomaly data sets with one  $\underline{x}_{nm}$  set associated with a certain set of anomaly errors. The CPU time for the harmonic analysis of 64,800 1°x1° anomalies to estimate two potential coefficient sets up to degree NN=250 was only 1 min. 26 sec. on an Amdahl 470 V/8 computer. This step of computing the potential coefficients may be termed as step 4.

There were two additional steps of the comparison of potential coefficient sets by degree, and of computing error estimates by degree and cumulatively for the undulations and anomalies implied by a coefficient set. These may be termed as steps 5 and 6, and are discussed in Sections 5 and 6 respectively.

The various steps in the algorithm for optimal estimation of coefficients are summarized in Table 3.4.

Table 3.4 Algorithm for Optimal Estimation of Potential Coefficients from  $1^\circ \times 1^\circ$  Global Anomaly Data.

Step #	Purpose	Input	Output	Reference	Remarks
1A	Integrals of Assoc. Legendre Fn.		45,451 values in each $1^\circ$ latitude band $0^\circ \leq \theta_i \leq 89^\circ$	Sec. 3.1	$N_{\max} = 300$
1B	Integrals of Assoc. Legendre Fn. $P_{lhm}$	Step 1A	$0^\circ \leq \theta_i \leq 179^\circ$	Sec. 3.1, eq. (3.3)	
1C	Modified Integrals of Assoc. Legendre Fn. $I_{lhm}$	Step 1B	$0^\circ \leq \theta_i \leq 179^\circ$	Sec. 3.1, eq. (3.4)	Based on $C_n$
2	Generation of Normals $r_{lhp}$	Step 1C	$180 \times (NN+1) \times 90$	Sec. 3.2	Large CPU time based on highest degree NN
3A	Reordering of Normals $R(m)$	Step 2	$180 \times 180 \times (NN+1)$	Sec. 3.31	
3B	Reordering of R.H.S. vectors $k_{nm}$	Step 1C	$90 \times (NN+1) \times (NN+2) / 2$	Sec. 3.32	
3C	Solution of Normals $\lambda_{nm}, ET$	Steps 3A, 3B, $\sigma_{\Delta g}$	$180 \times (NN+1) \times (NN+2) / 2$ $\times I_{lhm}$ $\sigma_{nm}^\alpha$ $(NN+1) \times (NN+2) / 2$	Sec. 3.33	Based on $\sigma_i^2(\Delta g)$ Large CPU time based on NN
4	Computation of Potl. Coeff. $C_{nm}^\alpha$	Step 3C, Global $1^\circ \times 1^\circ \Delta g$	$(NN+1)^2$	Sec. 3.4	Based on global $1^\circ \times 1^\circ \Delta g$
5	Comparison of Potl. Coeff. Sets	Step 4	Comparison Statistics	Sec. 5	
6	Statistics on P.C. and Error Est.	Step 3C	P.C. & Error Statistics	Sec. 6	

#### 4. POTENTIAL COEFFICIENT AND GRAVITY ANOMALY DATA SETS

The parameters affecting the optimal estimation of coefficients are given in the last column of Table 3.4. The highest degree  $N_{max}$ , to which the summations are carried out for computing the Fourier transforms of the covariances of  $1^\circ \times 1^\circ$  anomalies in (3.2), was kept as 300 based on experiments carried out by Colombo (1981, Sec. 4.2). The global anomaly degree variance model used by Colombo (ibid., Sec. 3.1) was also retained. It consisted of empirically obtained anomaly degree variances up to degree 100 from a  $180 \times 180$  potential coefficients field developed by Rapp in 1978, and by a two component variance model described by Rapp (1979, p. 15, Table 5, Case 1) for degree  $n > 100$ :

$$c_n = (n-1) \left[ \frac{\alpha_1}{n+A} (s_1)^{n+2} + \frac{\alpha_2}{n+B} \cdot \frac{1}{n-2} (s_2)^{n+2} \right] (\text{mgals})^2 \quad (4.1)$$

$$\alpha_1 = 3.4050, \alpha_2 = 140.03, s_1 = 0.998006, s_2 = 0.914232, A = 1, B = 2$$

The other parameters, and data sets, used in the optimal estimation of coefficients are described below.

##### 4.1 Anomaly Error Estimates

Several different sets of anomaly error estimates were used. One set computed average variance,  $\sigma_i^2$  in (2.32), in each latitude band from error estimates of a global  $1^\circ \times 1^\circ$  anomaly data set utilizing terrestrial anomalies merged with anomalies determined from Seasat data, and balance anomalies computed from potential coefficients being assigned standard error of 30 mgals. This anomaly data set was a slightly updated version, with some additional terrestrial data, of the set described in Section 2.3. The computed values of average anomaly standard errors,  $\sigma_i$ , per latitude band are given in Table 4.1, and this will be termed as anomaly error estimate A. The standard errors range from 30 to about 4 mgals.

Table 4.1 Average Anomaly Errors in  $1^\circ$  Latitude Bands for Error Estimate A.

Latitude Bands $i$	Average Anomaly Standard Error, $\sigma_i$ , in mgals														
0 to 14	30	27	27	27	27	27	28	27	27	26	25	25	24	23	22
15 to 29	22	21	20	19	19	16	16	15	16	16	15	15	15	15	14
30 to 44	12	12	11	11	11	11	11	11	10	11	10	9.9	10	10	11
45 to 59	11	11	11	11	12	12	11	11	12	12	10	10	10	11	10
60 to 74	11	10	9.8	10	9.9	10	10	9.2	9.4	9.7	9.7	8.9	9.3	8.3	8.1
75 to 89	6.9	7.1	8.3	8.5	8.9	9.1	8.8	8.8	8.8	9.1	8.8	7.5	7.6	7.9	7.4
90 to 104	8.0	8.2	8.4	8.4	8.9	9.1	8.7	8.3	8.7	7.7	7.3	7.3	7.7	7.4	7.6
105 to 119	8.1	7.4	7.4	7.8	7.2	7.6	7.2	6.8	6.9	6.5	6.4	6.0	5.6	5.7	5.8
120 to 134	5.6	5.3	5.0	4.2	4.6	3.8	4.1	3.9	4.6	4.9	4.1	4.1	4.4	4.8	5.2
135 to 149	4.4	4.0	3.6	3.9	4.4	5.1	5.0	4.4	4.5	4.6	3.8	3.6	3.3	3.7	5.5
150 to 164	3.7	3.9	4.5	5.2	5.9	6.7	8.0	11	12	13	27	28	27	28	28
165 to 179	26	26	25	24	24	24	24	24	23	25	26	26	23	14	14

A second set, termed anomaly error estimate B, assigned uniformly for each  $1^\circ$  latitude band average anomaly standard error,  $\sigma_j$ , of 5 mgals. Error estimate A is a realistic estimate of the current averaged anomaly variances in  $1^\circ$  latitude bands for  $1^\circ \times 1^\circ$  anomalies. Error estimate B assumes no latitude variation in averaged variances, and is therefore an idealized version of anomaly error distribution. A value of 5 mgals is an optimistic estimate giving a lower error bound till the Geopotential Research Mission is flown at the end of this decade.

A uniform average anomaly standard error of 20 mgals was also used in some tests, as a 20 mgal error was used for each anomaly in generating the current Rapp (1981) coefficients, as discussed at the end of Section 2.3 of this study. Another set of error estimates was developed on the same lines as error estimate A, but only using terrestrial data resulting in a range of average standard error,  $\sigma_j$ , from 30 to 9 mgals. Some other anomaly error estimates would be described in the tests in Sections 5.1 and 5.2.

#### 4.2 Data Sets A

The development of the current set of merged potential coefficients to degree and order 180 (Rapp, 1981) was described in Section 2.3. This will be termed as coefficient set A, and will be compared with other coefficient sets developed by optimal estimation.

Coefficient set A was used to compute a global set of 64,800  $1^\circ \times 1^\circ$  mean gravity anomalies by (2.11) using subroutine SSYNTH, with  $\gamma=979,800$  mgals. This global set will be termed as anomaly set A. As the maximum degree,  $N_{max}$ , in the summation in (2.11) was 180, the anomaly set A can only be used for estimating coefficients to the highest degree NN of 180. But the anomaly set A would be a good data set to test the effect of anomaly error estimates on the optimal estimation of coefficients, by testing the latter against coefficient set A. These tests will be described in Section 5.1.

#### 4.3 Data Sets B

Anomaly set B was the global set of 64,800  $1^\circ \times 1^\circ$  'adjusted anomalies' described in Section 2.3 obtained by implementing (2.38). Anomaly set B therefore retains the high degree ( $n > 180$ ) information present in the terrestrial and the Seasat altimeter derived anomalies, which were used to develop the 'adjusted anomalies'.

As mentioned in Section 2.3, the coefficient set developed by the harmonic analysis of anomaly set B, by implementing (2.5) with de-smoothing factors (2.7), using subroutine HARMIN will be termed as coefficient set B. Coefficient set B would be considered only up to degree and order 180.

Coefficient sets A and B are the same from degree 49 to 180. 'Adjusted SET1' coefficients, complete to degree and order 36, with some additional coefficients to degree 48, replaced the corresponding coefficients in coefficient set B to form the coefficient set A. The difference between these two sets is shown in Table 5.1.

The coefficients developed by optimal estimation from anomaly set B are therefore comparable to coefficient set B through degrees 2 to 180, or to coefficient set A through degrees 49 to 180. The comparison with coefficient set A through degrees 2 to 48 would also show the additional, though small, effect due to the simplified adjustment model in (2.35).

## 5. COMPARISON OF SETS OF POTENTIAL COEFFICIENTS

If the potential coefficients in two different estimates to degree NN are denoted by  $(\bar{C}_{nm}, \bar{S}_{nm})$  and  $(\bar{C}'_{nm}, \bar{S}'_{nm})$ , then the two sets of estimates may be compared in magnitude by percentage coefficient difference ( $\% \Delta_n$ ) by degree n, undulation difference ( $\sqrt{\Delta \ell_n}$ ) by degree, and anomaly difference ( $\sqrt{\Delta c_n}$ ) by degree.

$$\% \Delta_n = \frac{\Delta \sigma_n}{\sigma_n} \cdot 100 \quad (5.1)$$

$$\sigma_n^2 = \sum_{m=0}^n (\bar{C}_{nm}^2 + \bar{S}_{nm}^2) \quad (5.2)$$

$$\Delta \sigma_n^2 = \sum_{m=0}^n [(\bar{C}_{nm} - \bar{C}'_{nm})^2 + (\bar{S}_{nm} - \bar{S}'_{nm})^2] \quad (5.3)$$

$$\sqrt{\Delta \ell_n} = R \cdot \Delta \sigma_n \text{ meters} \quad (5.4)$$

$$\sqrt{\Delta c_n} = \gamma(n-1) \cdot \Delta \sigma_n \text{ mgals} \quad (5.5)$$

where, as before,  $\gamma = 979,800$  mgals is the average value of gravity over the whole globe approximated by a sphere of radius  $R=6.371 \times 10^6$  meters. For example, coefficient sets A and B differ up to degree 36; differ in some additional coefficients up to degree 48, and are the same in higher degrees to 180. This comparison is shown in Table 5.1.

Table 5.1 Comparison of Potential Coefficient Sets A and B (Sec. 4.2 and 4.3).

Degree n	% Coefficient Difference $\% \Delta_n$	Undulation Difference $\sqrt{\Delta \ell_n}$ in meters	Anomaly Difference $\sqrt{\Delta c_n}$ in mgals
2	1.23	.22	.03
3	.34	.06	.02
4	.39	.04	.02
5	.64	.05	.03
6	.51	.03	.02
9	.54	.01	.02
12	.56	.01	.01
24	.51	.00	.01
36	.71	.00	.01
37	.03	.00	.00
42	.17	.00	.00
48	.06	.00	.00
49-180	.00	.00	.00

## 5.1 Initial Tests with Data Set A

We first show in the first set of columns in Table 5.2, a comparison between coefficient set A and another coefficient set computed to degree 180 by harmonic analysis of the anomaly set A by HARMIN in (2.5), using de-smoothing factors in (2.7). The differences would arise primarily due to sampling error because of using  $1^\circ \times 1^\circ$  anomaly blocks of a finite size, instead of using an infinite number of point anomalies implied by the integral in (2.2). Additional differences would also arise due to any inadequacy in the de-smoothing factors, particularly a discontinuity in (2.7) near degree  $N/3=60$ , which is seen in Table 5.2. We also see an increase in the sampling error with higher degrees. Anomaly error estimates are, of course, not considered in (2.5).

In the next two sets of columns in Table 5.2, coefficient set A is compared with coefficient sets developed from anomaly set A by optimal estimation procedure, using error estimate B ( $\sigma_j=5$  mgals), and error estimate A ( $\sigma_j$  ranging from 30 to 4 mgals in Table 4.1) respectively. We would now see, besides the effect of sampling error, larger differences because of propagated noise of the anomalies. We would also expect that the larger the uncertainty in anomaly error estimate, the larger would be the difference from coefficient set A. We do, in fact, see increased differences in the second set of columns over the first set of columns, and further increased differences in the third set of columns over the second set. However, we do not find any discontinuity in the optimal estimation procedure in the second and third sets of columns near degree 60, as is seen in the first set of columns with de-smoothing factors.

**Table 5.2** Variation of Coefficients from De-smoothing Factors with Coefficients from Optimal Estimation.  
Comparison of Coefficient Set A with 3 Coefficient Sets Obtained from Anomaly Set A.

Degree n	De-smoothing Factors (2.7) with (2.5)			Optimal Estimation Procedure (Table 3.4)					
	Anomaly Errors Not Considered Directly			Anomaly Error Estimate B**			Anomaly Error Estimate A**		
	% $\Delta_n$	$\sqrt{\Delta l_n}$ m	$\sqrt{\Delta c_n}$ mgal	% $\Delta_n$	$\sqrt{\Delta l_n}$ m	$\sqrt{\Delta c_n}$ mgal	% $\Delta_n$	$\sqrt{\Delta l_n}$ m	$\sqrt{\Delta c_n}$ mgal
2	.61	.11	.02	.64	.11	.02	.85	.15	.02
3	.44	.08	.03	.48	.09	.03	.40	.08	.02
6	.56	.03	.02	.58	.03	.03	.63	.04	.03
12	.91	.01	.02	.87	.01	.02	1.4	.02	.03
36	1.2	.00	.02	1.7	.00	.02	5.0	.01	.07
60	2.1	.00	.04	2.3	.00	.04	6.9	.01	.13
61	4.4	.01	.07	2.9	.01	.05	8.6	.02	.14
90	8.9	.01	.14	6.0	.01	.10	15.2	.02	.25
120	14.2	.01	.23	10.7	.01	.17	21.4	.02	.34
150	22.3	.01	.30	22.2	.01	.30	33.9	.02	.45
180	27.4	.01	.35	36.2	.02	.46	46.8	.02	.60

\*Anomaly errors were not considered in computing coefficients from anomalies using de-smoothing factors.

\*\*Error Estimate B:  $\sigma_j$  in (2.32) = 5 mgals.

Error Estimate A:  $\sigma_j$  ranges from 30 to 4 mgals, see Table 4.1.

**Table 5.3** Variation of Optimally Estimated Coefficients with Variation in Anomaly Error Estimates. Comparison of Coefficient Set A with 6 Coefficient Sets Estimated from Anomaly Set A.

Degree n	Case 1 $\sigma_i = .001$ mgal			Case 2 $\sigma_i = 1$ mgal			Case 3* $\sigma_i = 5$ mgal			Case 4* $\sigma_i = 30$ to 4 mgal			Case 5 $\sigma_i = 30$ to 9 mgal			Case 6 $\sigma_i = 20$ mgal		
	% $\Delta n$	$\sqrt{\Delta \rho} n$ m	$\sqrt{\Delta C} n$ mgal	% $\Delta n$	$\sqrt{\Delta \rho} n$ m	$\sqrt{\Delta C} n$ mgal	% $\Delta n$	$\sqrt{\Delta \rho} n$ m	$\sqrt{\Delta C} n$ mgal	% $\Delta n$	$\sqrt{\Delta \rho} n$ m	$\sqrt{\Delta C} n$ mgal	% $\Delta n$	$\sqrt{\Delta \rho} n$ m	$\sqrt{\Delta C} n$ mgal	% $\Delta n$	$\sqrt{\Delta \rho} n$ m	$\sqrt{\Delta C} n$ mgal
2	.61	.11	.02	.61	.11	.02	.64	.11	.02	.85	.15	.02	.78	.14	.02	1.10	.20	.03
3	.45	.08	.03	.48	.09	.03	.48	.09	.03	.40	.08	.02	.44	.08	.03	.52	.10	.03
4	.45	.04	.02	.45	.04	.02	.46	.04	.02	.44	.04	.02	.51	.05	.02	.65	.06	.03
5	.81	.06	.04	.92	.07	.04	.93	.07	.04	.82	.06	.04	.98	.07	.04	1.14	.08	.05
6	.56	.03	.02	.56	.03	.02	.58	.03	.03	.63	.04	.03	.88	.05	.04	1.05	.06	.05
9	.71	.02	.02	.77	.02	.03	.79	.02	.03	.67	.02	.02	.97	.03	.03	1.90	.05	.06
10	.62	.01	.02	.62	.01	.02	.67	.02	.02	.90	.02	.03	1.10	.02	.03	2.16	.05	.07
11	1.07	.02	.03	.68	.01	.02	.68	.01	.02	.72	.01	.02	1.14	.02	.03	2.53	.04	.07
12	.83	.01	.01	.83	.01	.01	.87	.01	.02	1.44	.02	.03	2.71	.03	.05	5.63	.06	.10

\*Cases 3 and 4 correspond to Anomaly Error Estimates B and A respectively in Table 5.2. Results in Table 5.3 are also valid for coefficients estimated to higher degrees, as estimated coefficients are not correlated.

To examine, in greater detail, the effect of anomaly error estimates on coefficients by optimal estimation, several different sets of coefficients were computed with anomaly error estimates as shown in Table 5.3, which also shows the comparison with coefficient set A. There is some instability in the inverse of matrix  $(R(m)+W)$  in (2.30), when the elements of diagonal matrix  $W$  in (2.32) correspond to  $\sigma_i$  of .001 mgals. But with  $\sigma_i \geq 1$  mgal, Table 5.3 shows conclusively that optimally estimated coefficients depend on the magnitude of anomaly error estimates.

The tests in Table 5.3 were run with  $NN=12$ , after ensuring that the estimated coefficients are not correlated, and hence the results in Table 5.3 with  $NN=12$  are also valid for higher degrees. This conclusion was arrived at by repeating the optimal estimation of coefficients for anomaly set A, with both error estimates A and B, for  $NN=180$  in Table 5.2, also for  $NN=60$  and  $NN=12$ . The common coefficients were the same whether the coefficients were estimated to  $NN=12$ , 60, or 180. Similar results were obtained later with anomaly set B.

## 5.2 Initial Tests with Data Set B

Tests were first made to examine the variation in optimally estimated coefficients from anomaly set B by using different error estimates as in Table 5.3, and comparing the optimally estimated coefficients against the coefficient set B. The results were similar to those presented in Table 5.3 showing larger variation in the optimally estimated coefficients as larger anomaly error estimates were used, reflecting the effect of propagated anomaly errors.

It was also noticed that generally there was a better agreement between coefficient set B and optimally estimated coefficients from anomaly set B for any given anomaly error estimate, as contrasted with the case of agreement between coefficient set A and optimally estimated coefficients from anomaly set A presented in Section 5.1. For example, this may be seen in Table 5.4 for the anomaly error estimates for  $\sigma_i = 5$  mgals, and  $\sigma_i = 1$  mgal, when contrasted with similar results in Table 5.3. This may be due to the anomalies in set B having been obtained in a combined adjustment with 'SET1' coefficients (Section 2.3), yielding the anomaly set B and the 'adjusted SET1' coefficients. The adjustment of anomalies in set B not only adjusts the anomaly spectrum to degree 36 (including some coefficients to 48), but perhaps also modifies to some extent the higher degree spectrum. This will be seen in the results in Section 5.4.

However, we also find curiously a larger disagreement in the comparisons in Section 5.2 at the very low degrees, when contrasted with the comparisons in Section 5.1. This may be seen again in Table 5.4 for the anomaly error estimates for  $\sigma_i = 5$  mgals, and  $\sigma_i = 1$  mgal, when contrasted with similar results in Table 5.3 for degrees 2 and 3. This may be due to the simplified adjustment model in (2.35) and (2.36) being generally adequate at degrees greater than 3. Or, this may be an artifact of forcing the weight matrix of anomalies in (2.37) as  $\cos \phi' / \sigma^2$ , while the weight matrix in optimal estimation is implicitly  $1/\sigma_i^2$  in (2.30), read with (2.32).

Several sets of coefficients were then optimally estimated with  $\sigma_i$  being modified from 1 mgal to  $1/\cos \phi_i'$  mgal, and  $1/\sqrt{\cos \phi_i'}$  mgal to match the anomaly weights in (2.37) as  $\cos \phi' / \sigma^2$ . However, this made the agreement with coefficient set B worse for all degrees as compared to the case of  $\sigma_i = 1$  mgal. Other sets

**Table 5.4** Agreements in Data Sets B Compared with Agreements in Data Sets A (Table 5.3).  
Comparison of Coefficient Set B with 4 Coefficient Sets Estimated from Anomaly Set B.

Degree n	$\sigma_j = 5 \text{ mgal}^*$			$\sigma_j = 1 \text{ mgal}^{**}$			$\sigma_j = 1 \cdot \cos \phi_j \text{ mgal}$			$\sigma_j = 1 \cdot \sqrt{\cos \phi_j} \text{ mgal}$		
	% $\Delta n$	$\sqrt{\Delta \xi \eta}$ m	$\sqrt{\Delta C \eta}$ mgal	% $\Delta n$	$\sqrt{\Delta \xi \eta}$ m	$\sqrt{\Delta C \eta}$ mgal	% $\Delta n$	$\sqrt{\Delta \xi \eta}$ m	$\sqrt{\Delta C \eta}$ mgal	% $\Delta n$	$\sqrt{\Delta \xi \eta}$ m	$\sqrt{\Delta C \eta}$ mgal
2	4.89	.87	.13	4.89	.87	.13	9.79	1.74	.27	7.83	1.39	.21
3	3.59	.68	.21	3.59	.68	.21	8.08	1.53	.47	6.15	1.16	.36
4	.52	.05	.02	.52	.05	.02	.71	.07	.03	.04	.00	.00
5	.92	.07	.04	.92	.07	.04	1.53	.11	.07	.06	.00	.00
6	.20	.01	.01	.20	.01	.01	.09	.01	.00	.02	.00	.00
9	.30	.01	.01	.28	.01	.01	.10	.00	.00	.07	.00	.00
10	.16	.00	.01	.10	.00	.00	.06	.00	.00	.06	.00	.00
11	.34	.01	.01	.23	.00	.01	.11	.00	.00	.11	.00	.00
12	.45	.00	.01	.14	.00	.00	.10	.00	.00	.10	.00	.00

\*Comparable to Case 3 in Table 5.3.

\*\*Comparable to Case 2 in Table 5.3.

The third and fourth cases in Table 5.4 were tried to reduce the disagreements in the second case. The disagreements were reduced to degree 5, and degree 3, respectively in the third and fourth cases.

of coefficients were then optimally estimated with  $\sigma_j = 1 \cdot \cos \phi_j^i$  mgal, and  $1 \cdot \sqrt{\cos \phi_j^i}$  mgal. The last case resulted in close agreement with coefficient set B at degrees greater than 3, but the disagreement persisted at degrees 2 and 3, and was now of a larger amount. All these tests were run with coefficients estimated to degree NN=12.

Table 5.4 shows the comparison of coefficient set B with four optimally estimated coefficient sets by harmonic analysis of anomaly set B. The anomaly error estimates in the four cases were  $\sigma_j = 5, 1, 1 \cdot \cos \phi_j^i$  and  $1 \cdot \sqrt{\cos \phi_j^i}$  mgal. The first two cases are for comparison with similar cases in Table 5.3 for the data set A, and the last two cases in Table 5.4 were an attempt to reduce the disagreements at degrees 2 and 3. The tests were repeated with data sets A in Section 5.1 with  $\sigma_j = 1/\cos \phi_j^i, 1/\sqrt{\cos \phi_j^i}, 1, 1 \cdot \cos \phi_j^i$ , and  $1 \cdot \sqrt{\cos \phi_j^i}$  but did not show any larger differences as noticed in the case of data sets B.

As already mentioned, the optimally estimated coefficients from the adjusted anomalies in set B, adjusted through the simplified model in (2.35), show generally a better agreement with coefficient set B as contrasted with the agreements of data sets A in Section 5.1, except for degree 2 and 3. Coefficient sets will be optimally estimated from anomaly set B to higher degrees up to NN=250 in Section 5.4 for the cases of anomaly error estimates A and B, without forcing these error estimates to  $\sigma_j \sqrt{\cos \phi_j^i}$  or  $\sigma_j / \sqrt{\cos \phi_j^i}$ .

### 5.3 Test with Altered Anomaly Data Set

The assembling of 64,800  $1^\circ \times 1^\circ$  global anomalies was described in Section 2.3, where 8049 anomalies were assigned values implied by 'SET1' coefficients (complete to degree 36), and a standard error of 30 mgals. During the combined adjustment of anomalies and SET1 coefficients, anomalies with higher standard errors received larger corrections. The location of 3827 anomalies, which had corrections larger than 7 mgals, were shown in Rapp (1981, p. 25, Fig. 6) and is now reproduced here as Figure 5.1.

Four  $10^\circ \times 10^\circ$  blocks are marked in Figure 5.1, two each in the northern hemisphere in Central Siberia and Central Africa, and two each in the southern hemisphere in Southwest Africa and Central Andes in South America. The latitudinal and longitudinal limits of these blocks are listed in Table 5.6. Three tests were made to examine the effect on optimally estimated coefficients if some  $1^\circ \times 1^\circ$  anomalies in the global anomaly data are set to zero instead of the value implied by a-priori coefficients. From the global anomaly set A, three other anomaly sets were obtained: anomaly set 1 with 200  $1^\circ \times 1^\circ$  anomalies set to zero in the two  $10^\circ \times 10^\circ$  blocks in the northern hemisphere; anomaly set 2 with 200  $1^\circ \times 1^\circ$  anomalies set to zero in the two  $10^\circ \times 10^\circ$  blocks in the southern hemisphere; and anomaly set 3 with 400  $1^\circ \times 1^\circ$  anomalies set to zero in the four  $10^\circ \times 10^\circ$  blocks in both hemispheres. Four sets of coefficients were optimally estimated, all to degree NN=60, from the global anomaly sets A, 1, 2, and 3. The realistic anomaly error estimate A,  $\sigma_j = 30$  to 4 mgals in Table 4.1, was used in all four cases. The comparison of coefficient set A with these 4 sets of coefficients is shown in Table 5.5.

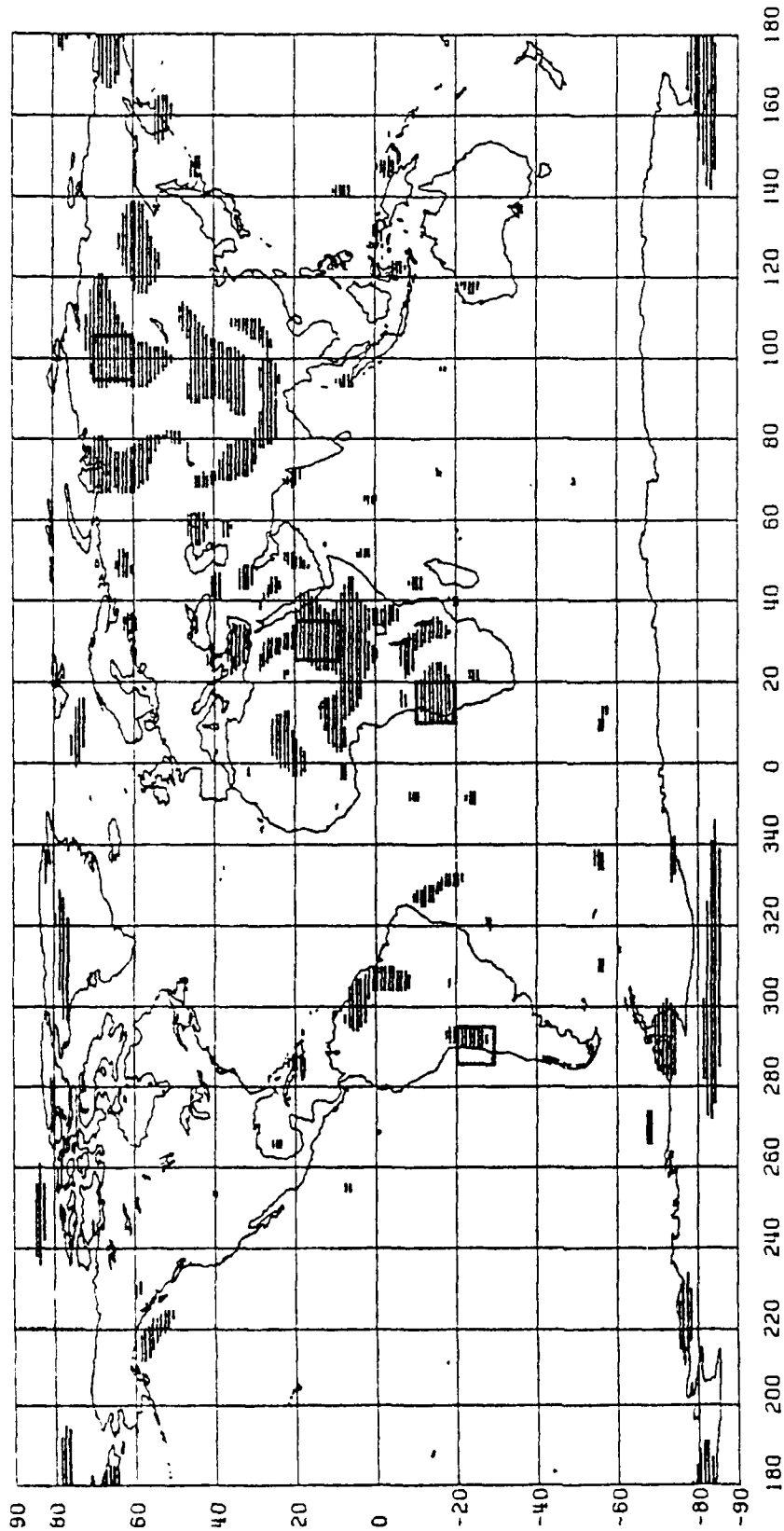


**Figure 5.1** Location of Four  $10^\circ \times 10^\circ$  Blocks where  $1^\circ \times 1^\circ$  Anomalies were set to Zero in Anomaly Set A. (Figure Reproduced from Rapp (1981, p. 25, Fig. 6) showing locations of 3827  $1^\circ \times 1^\circ$  Anomalies where Residuals after Adjustment were Greater Than 7 mgals).

Figure 6.3

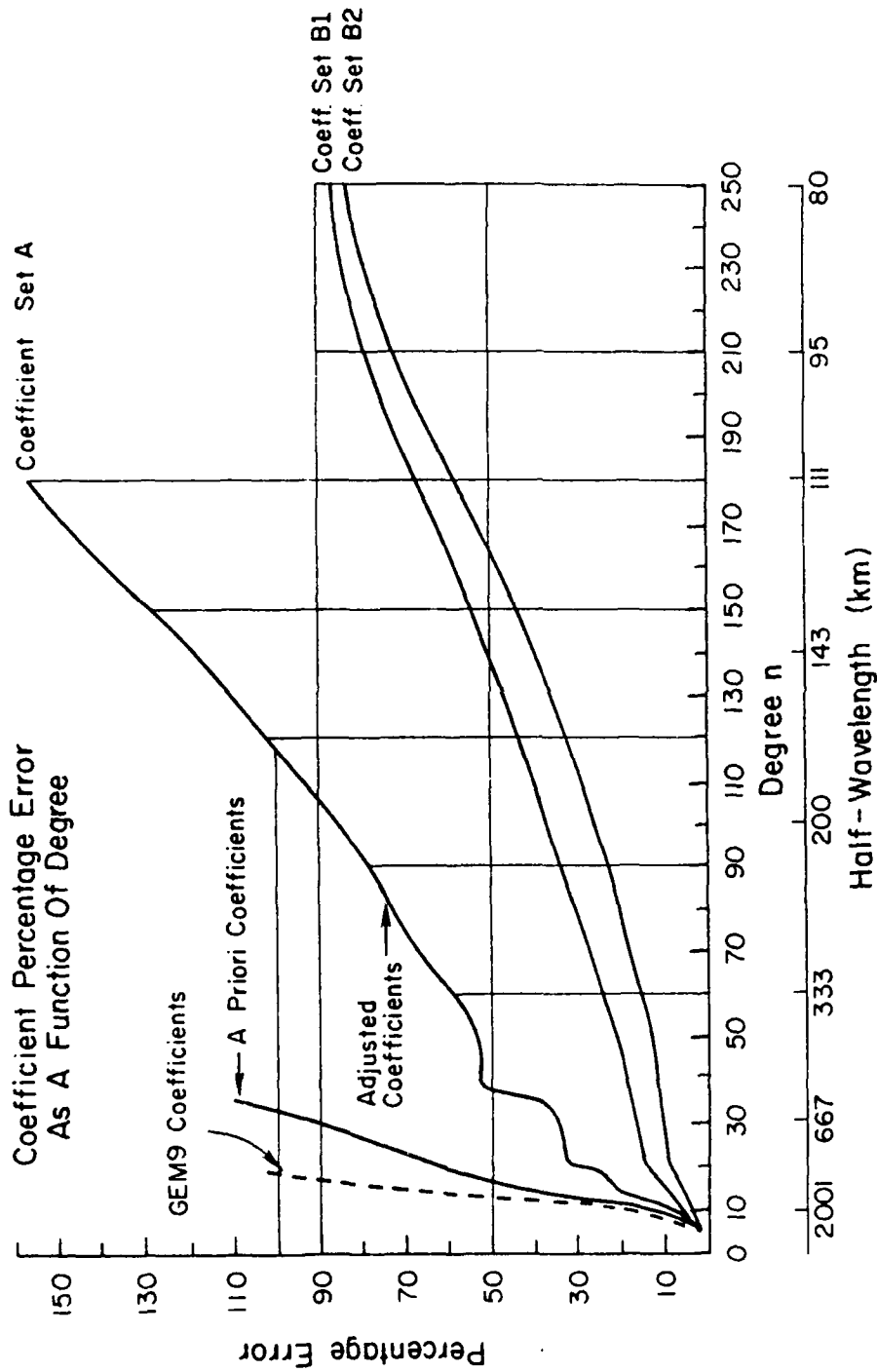


(Figure Reproduced from Rapp (1981, p. 33, Fig. 11) on which additional curves have been drawn for Coefficient Sets B1 and B2.)

**Table 6.3** Coefficient Percentage Error Estimates per Degree by Optimal Estimation. Variation Due to Anomaly Error Estimates.

Degree n	Coefficient Set B1			Coefficient Set B2		
	Anomaly Error Estimate A			Anomaly Error Estimate B		
	Sampling %S <sub>n</sub>	Noise %N <sub>n</sub>	Total %T <sub>n</sub>	Sampling %S <sub>n</sub>	Noise %N <sub>n</sub>	Total %T <sub>n</sub>
2	0.2	3.1	3.1	0.03	1.8	1.8
3	0.1	1.8	1.8	0.01	1.0	1.0
6	0.2	3.3	3.3	0.04	1.8	1.8
12	1.5	11.3	11.4	0.4	6.4	6.4
24	3.2	16.2	16.6	0.9	9.3	9.3
36	4.3	18.8	19.2	1.2	10.8	10.9
60	7.0	23.0	24.0	3.0	13.6	13.9
90	17.3	31.1	35.6	12.5	19.4	23.1
120	27.2	34.0	43.5	22.5	22.0	31.5
150	41.7	36.1	55.2	37.1	24.6	44.5
180	57.8	35.0	67.5	53.8	24.8	59.3
210	71.9	31.2	78.3	68.9	22.9	72.6
240	82.4	26.1	86.4	80.1	19.7	82.5
250	84.9	24.5	88.4	82.9	18.7	85.0

Both coefficient sets B1 and B2 estimated from anomaly set B using anomaly error estimates A and B respectively. Error Estimate A :  $\sigma_j$  ranges from 30 to 4 mgals (Table 4.1). Error Estimate B :  $\sigma_j = 5$  mgals.

## 6.2 Error Estimates by Degree

The expression for error variances of a coefficient,  $\bar{c}_{nm}^\alpha$ , due to sampling error,  $[E_s]_{\bar{c}_{nm}^\alpha}$ , propagated noise,  $[E_n]_{\bar{c}_{nm}^\alpha}$ , and the total variance,  $\sigma_{nm\alpha}^2$ , were given in (3.10), (3.9) and (3.8) respectively. We may now define the error variances per degree due to sampling,  $\sigma_{\epsilon sn}^2$ , due to propagated noise,  $\sigma_{\epsilon nn}^2$ , and the total error variance  $\sigma_{\epsilon n}^2$  per degree, as:

$$\begin{pmatrix} \sigma_{\epsilon sn}^2 \\ \sigma_{\epsilon nn}^2 \\ \sigma_{\epsilon n}^2 \end{pmatrix} = \sum_{m=0}^n \sum_{\alpha=0}^1 \begin{pmatrix} [E_s]_{\bar{c}_{nm\alpha}} \\ [E_n]_{\bar{c}_{nm\alpha}} \\ [E_T]_{\bar{c}_{nm\alpha}} \end{pmatrix} \quad (6.1)$$

where we have used  $[E_T]_{\bar{c}_{nm\alpha}} \equiv \sigma_{nm\alpha}^2$  in view of (2.16), and  $[\cdot]$  indicates one element of the matrix. The errors (square root of variance) per degree,  $\sigma_{\epsilon sn}$ ,  $\sigma_{\epsilon nn}$ ,  $\sigma_{\epsilon n}$ , may be expressed as percentages of potential coefficient variation,  $\sigma_n$ , per degree in (3.11). If we denote these percentage errors due to sampling, noise and total as  $\%S_n$ ,  $\%N_n$ ,  $\%T_n$  per degree, then:

$$\begin{pmatrix} \%S_n \\ \%N_n \\ \%T_n \end{pmatrix} = \begin{pmatrix} \sigma_{\epsilon sn} \\ \sigma_{\epsilon nn} \\ \sigma_{\epsilon n} \end{pmatrix} \cdot \left(\frac{100}{\sigma_n}\right) \quad (6.2)$$

$$\text{with } \sigma_n = \sqrt{c_n / (\gamma(n-1))} \quad (6.3)$$

The percentage errors,  $\%S_n$ ,  $\%N_n$ ,  $\%T_n$ , have been tabulated in Table 5.3 for coefficient sets B1 and B2. We note that  $\%S_n$  is small at low degrees, but increases sharply with degree. The sampling error predominates after around degree 120, is more than 50% of the coefficient value at degree 180, and more than 80% of the coefficient value at degree 250. Because of the predominant effect of the sampling error at high degrees, we find that the total percentage error,  $\%T_n$ , is only slightly different for sets B1 and B2 at degree 250, though it is much smaller at lower degrees for set B2. However,  $\%T_n$  does not reach 100% in any case even at degree 250, because the optimal estimator cannot have a larger error than a null estimator (which will correspond to 100% error), (Colombo, 1981, p. 73).

Figure 6.2

COEFFICIENT SET B1

Anomaly Magnitude per Degree in mgal

$$\sqrt{c_n} = \gamma (n-1) * \sigma_n ; \sigma_n^2 = \sum_{m=0}^n [\bar{C}_{nm}^2 + \bar{S}_{nm}^2]$$

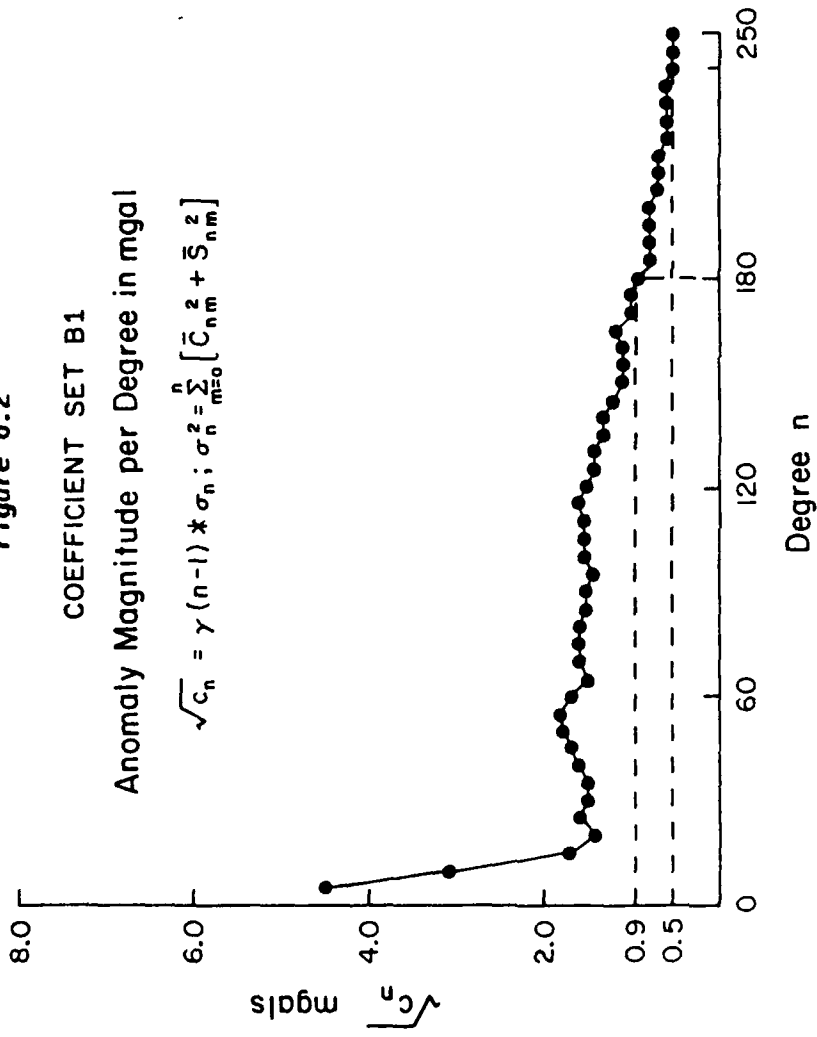
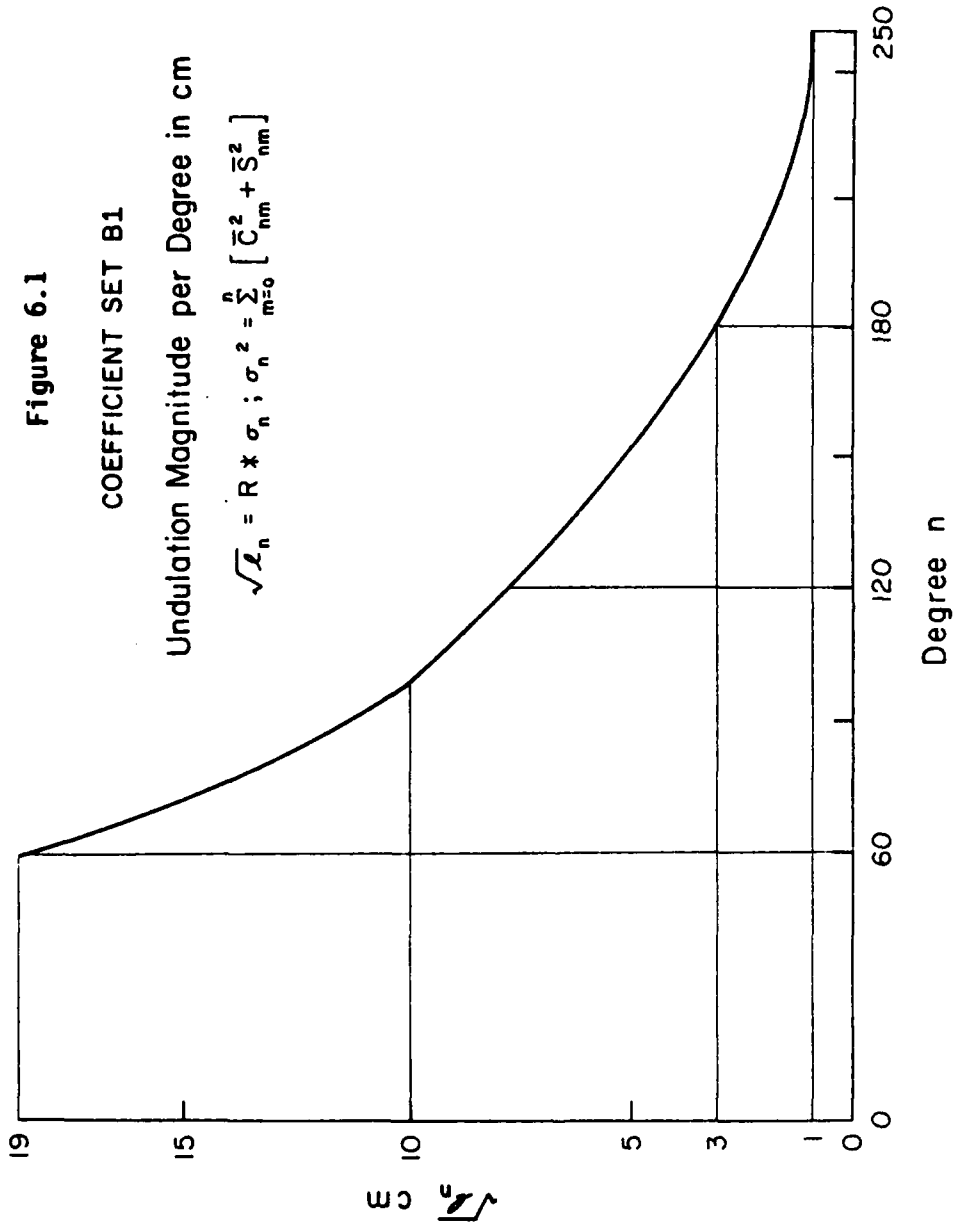


Figure 6.1

COEFFICIENT SET B1

Undulation Magnitude per Degree in cm

$$\sqrt{L}_n = R * \sigma_n ; \sigma_n^2 = \sum_{m=0}^n [\bar{C}_{nm}^2 + \bar{S}_{nm}^2]$$



**Table 6.2** Undulation and Anomaly Magnitudes per Degree and Cumulatively. Comparison of New and Current Sets of Potential Coefficients.

Degree n	Coefficient Set B1				Coefficient Set A			
	Anomaly Error Estimate A				Anomaly Errors Not Considered Directly			
	$\sqrt{\lambda n}$ m	$\frac{\sqrt{\Sigma \lambda n}}{n}$ m	$\sqrt{Cn}$ mgal	$\frac{\sqrt{\Sigma Cn}}{n}$ mgal	$\sqrt{\lambda n}$ m	$\frac{\sqrt{\Sigma \lambda n}}{n}$ m	$\sqrt{Cn}$ mgal	$\frac{\sqrt{\Sigma Cn}}{n}$ mgal
2	17.80	17.8	2.74	2.7	17.90	17.9	2.75	2.8
3	18.57	25.7	5.71	6.3	18.91	26.0	5.82	6.4
6	5.65	29.0	4.35	9.9	5.72	29.3	4.40	10.1
12	1.02	29.8	1.73	12.6	1.06	30.1	1.79	12.8
24	0.39	29.9	1.39	14.1	0.41	30.3	1.45	14.3
36	0.23	29.9	1.26	14.9	0.24	30.3	1.32	15.1
60	0.19	29.9	1.72	17.0	0.20	30.3	1.85	17.4
90	0.11	30.0	1.51	19.2	0.12	30.3	1.62	19.8
120	0.08	30.0	1.47	20.9	0.09	30.3	1.61	21.7
150	0.05	30.0	1.12	22.0	0.06	30.3	1.34	23.1
180	0.03	30.0	0.90	22.7	0.05	30.3	1.28	24.2
210	0.02	30.0	0.71	23.2				
240	0.01	30.0	0.54	23.4				
250	0.01	30.0	0.46	23.5				

Coefficient Set B1 estimated optimally from anomaly set B to degree 250 with anomaly error estimate A :  $\sigma_i$  ranging from 30 to 4 mgals (see Table 4.1).  
 Coefficient set A is the current set of coefficients (Rapp, 1981) to degree 180. (Also see Sec. 2.3).  
 Anomaly errors were not considered in computing coefficients from anomalies using de-smoothing factors.

**Table 6.1** Variation of Optimally Estimated Coefficients to Degree 250 with Variation in Anomaly Error Estimate.  
Comparison of Coefficient Set B1 with Coefficient Set B2.

Degree n	% Coefficient Difference $\% \Delta_n$	Undulation Difference $\sqrt{\Delta \xi_n}$ in meters	Anomaly Difference $\sqrt{\Delta c_n}$ in mgals
2	3.4	.61	.09
3	9.2	1.70	.52
6	4.0	.23	.17
12	10.5	.11	.18
24	6.6	.03	.09
36	4.4	.01	.06
60	5.5	.01	.09
90	11.7	.01	.18
120	14.6	.01	.22
150	20.2	.01	.23
180	26.8	.01	.24
210	30.6	.01	.22
240	37.0	.01	.20
250	40.6	.00	.19

Both coefficient sets B1 and B2 were estimated from anomaly set B to degree and order 250 using anomaly error estimates A and B respectively.

Error Estimate A :  $\sigma_i$  ranges from 30 to 4 mgals (see Table 4.1).

Error Estimate B :  $\sigma_i = 5$  mgals.

## 6. OPTIMAL ESTIMATION OF COEFFICIENTS TO DEGREE AND ORDER 250

As the anomaly set A was computed by (2.11) from coefficient set A to degree  $N_{\max}=180$ , it could not be used to compute coefficients beyond degree 180. Accordingly, anomaly set B was used to optimally estimate coefficients to degree  $NN=250$ , using both anomaly error estimates A and B. We will term these coefficient sets B1 and B2 respectively. As the anomaly error estimate A represents our current knowledge of  $1^\circ \times 1^\circ$  anomalies realistically, coefficient set B1 would represent the current estimates of high degree gravity field. However, comparisons with coefficient set B2 would give us the upper bound of improvement, with respect to anomaly error estimates, that we may expect until the end of this decade.

### 6.1 Magnitude Information by Degree

We first list in Table 6.1 the percentage coefficient difference, undulation difference, and anomaly difference by degree,  $\% \Delta_n$ ,  $\sqrt{\Delta \ell_n}$ ,  $\sqrt{\Delta c_n}$ , between coefficient sets B1 and B2. We notice large differences due to different anomaly error estimates A and B, as we would expect from the information to degree 180 in Table 5.7. The disagreement at degree 3 is particularly noticeable because of strong equatorial assymetry of error estimate A in Table 4.1.

We next list in Table 6.2, the undulation magnitude  $\sqrt{\ell_n}$ , and anomaly magnitude  $\sqrt{c_n}$  by degree n, and also cumulatively, for coefficient set B1 to degree 250. The same information is also listed for the current coefficient set A (Rapp, 1981) till degree 180.

The undulation, and anomaly magnitude, per degree, for coefficient set B1 have been plotted in Figures 6.1 and 6.2. The values of  $\sqrt{\ell_n}$  and  $\sqrt{c_n}$  at degree 250 are about 1 cm, and about 0.5 mgals respectively.

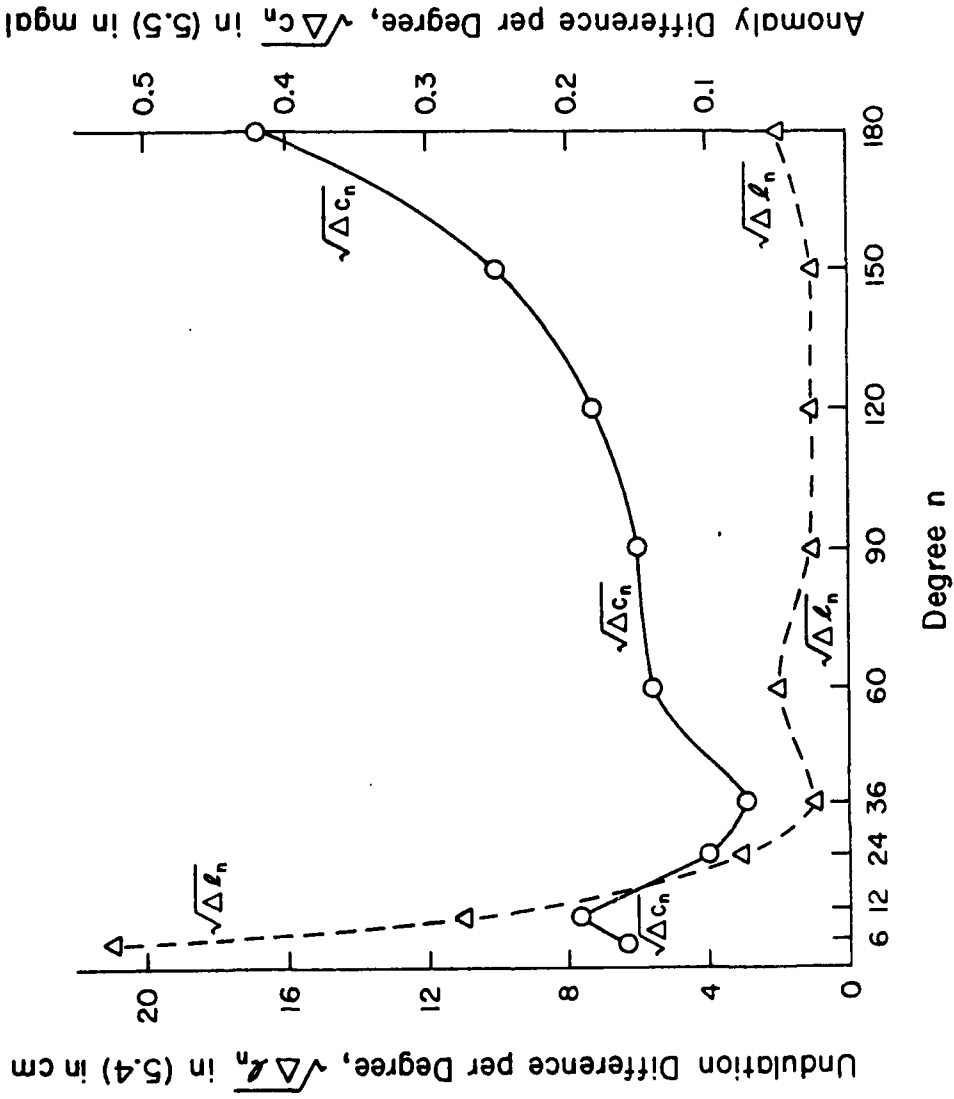
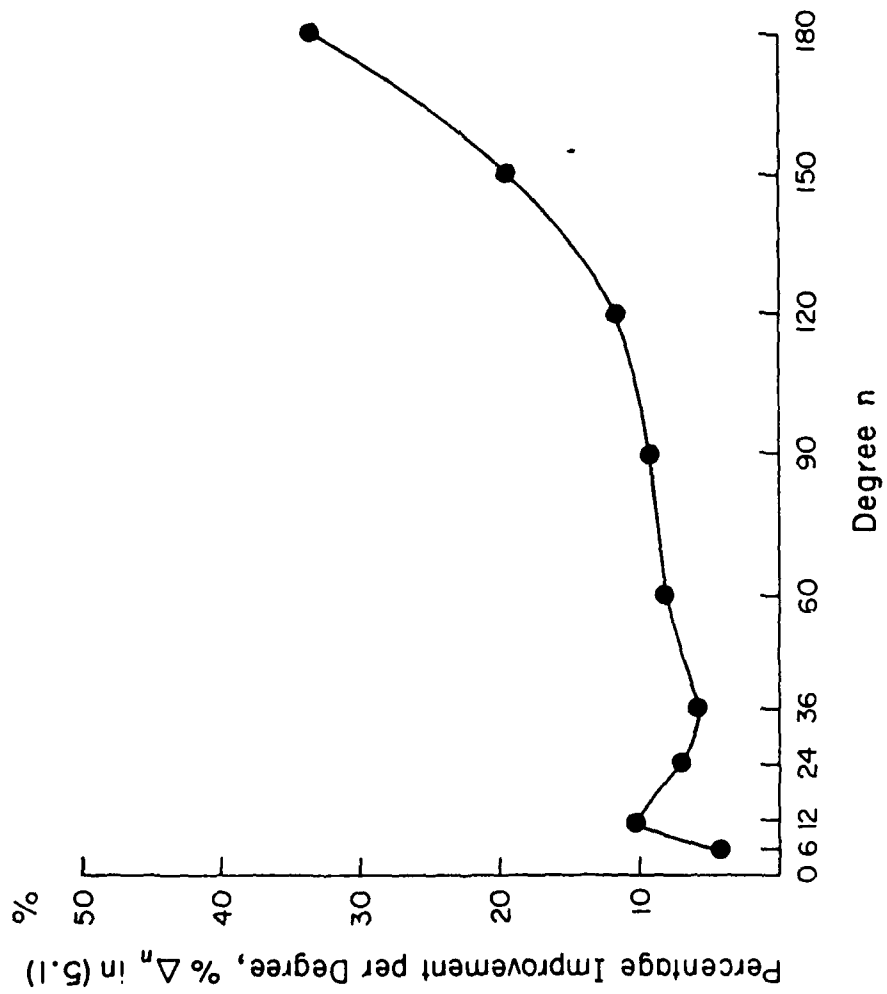


Figure 5.3 Improvement in Undulation and Anomaly per Degree Due to Optimal Estimation of Coefficients (Sec. 2.2) Over the Use of De-smoothing Factors (Sec. 2.1). Data Sets B. Error Estimate A (see Table 5.7).



**Table 5.7 Improvement Due to Optimal Estimation of Coefficients.  
Comparison of Both Coefficients Sets A and B, each with 4 Optimally Estimated Coefficient Sets  
from Anomaly Sets A and B Using Error Estimates A and B (Section 4).**

Degree n	Comparison with Coefficient Set A												Comparison with Coefficient Set B											
	Anomaly Set A						Anomaly Set B						Anomaly Set A						Anomaly Set B					
	Error Est. A		Error Est. B		Error Est. A		Error Est. B		Error Est. A		Error Est. B		Error Est. A		Error Est. B		Error Est. A		Error Est. B		Error Est. A		Error Est. B	
	% $\Delta\eta$	$\sqrt{\Delta\eta}$ m	$\sqrt{\Delta C\eta}$ mgal	% $\Delta\eta$	$\sqrt{\Delta\eta}$ m	$\sqrt{\Delta C\eta}$ mgal	% $\Delta\eta$	$\sqrt{\Delta\eta}$ m	$\sqrt{\Delta C\eta}$ mgal	% $\Delta\eta$	$\sqrt{\Delta\eta}$ m	$\sqrt{\Delta C\eta}$ mgal	% $\Delta\eta$	$\sqrt{\Delta\eta}$ m	$\sqrt{\Delta C\eta}$ mgal	% $\Delta\eta$	$\sqrt{\Delta\eta}$ m	$\sqrt{\Delta C\eta}$ mgal	% $\Delta\eta$	$\sqrt{\Delta\eta}$ m	$\sqrt{\Delta C\eta}$ mgal	% $\Delta\eta$	$\sqrt{\Delta\eta}$ m	$\sqrt{\Delta C\eta}$ mgal
2	.85	.15	.02	.64	.11	.02	2.0	.36	.06	3.8	.68	.11	1.4	.25	.04	1.2	.22	.03	2.5	.45	.07	4.9	.87	.13
3	.40	.08	.02	.48	.09	.03	5.4	1.02	.31	3.6	.69	.21	.18	.03	.01	.32	.06	.02	5.4	1.03	.32	3.6	.68	.21
6	.63	.04	.03	.58	.03	.03	3.8	.22	.17	.58	.03	.03	.23	.01	.01	.20	.01	.01	3.8	.21	.16	.20	.01	.01
12	1.4	.02	.03	.87	.01	.02	10.4	.11	.19	.74	.01	.01	1.2	.01	.02	.32	.00	.01	10.4	.11	.19	.45	.00	.01
24	3.9	.02	.06	1.2	.00	.02	7.0	.03	.10	1.3	.01	.02	3.6	.01	.05	.83	.00	.01	6.9	.03	.10	1.1	.00	.02
36	5.0	.01	.07	1.7	.00	.02	5.6	.01	.07	1.8	.00	.02	5.0	.01	.07	1.3	.00	.02	5.5	.01	.07	1.7	.00	.02
60	6.9	.01	.13	2.3	.00	.04	7.7	.02	.14	3.2	.01	.06	6.9	.01	.13	2.3	.00	.04	7.7	.02	.14	3.2	.01	.06
90	15.2	.02	.25	6.0	.01	.10	9.0	.01	.15	3.6	.00	.06	15.2	.02	.25	6.0	.01	.10	9.0	.01	.15	3.6	.00	.06
120	21.4	.02	.34	10.7	.01	.17	11.2	.01	.18	5.0	.00	.08	21.4	.02	.34	10.7	.01	.17	11.2	.01	.18	5.0	.00	.08
150	33.9	.02	.45	22.2	.01	.30	19.0	.01	.25	5.9	.00	.08	33.9	.02	.45	22.2	.01	.30	19.0	.01	.25	5.9	.00	.08
180	46.8	.02	.60	36.2	.02	.46	33.0	.02	.42	17.6	.01	.23	46.8	.02	.60	36.2	.02	.46	33.0	.02	.42	17.6	.01	.23

Error Estimate A :  $\sigma_j$  in (2.32) ranges from 30 to 4 mgals (Table 4.1).

Error Estimate B :  $\sigma_j = 5$  mgals.

See Section 4.2 for coefficient set A and anomaly set A.

See Section 4.3 for coefficient set B and anomaly set B.

anomaly error estimates are represented by error estimate A in Table 4.1. Hence, a slightly conservative estimate of current improvement in coefficients is represented by the comparison of coefficient B (by de-smoothing factors from anomaly set B) with the optimally estimated coefficients from anomaly set B using error estimate A. This improvement,  $\% \Delta_n$  in (5.1), is seen in Table 5.7 to be about 8% at degree 60, about 11% at degree 120, and rises to about 33% at degree 180. This improvement is also shown in Figure 5.2. The improvement by degree in geoid undulation difference  $\sqrt{\Delta \ell_n}$  in (5.4), and anomaly difference  $\sqrt{\Delta c_n}$  in (5.5) is shown in Figure 5.3. The improvements have been shown only to degree 180. The cumulative undulation difference, and the cumulative anomaly difference, to degree 180 was 1.51 meters and 2.70 mgal respectively.

$$\text{cumulative undulation difference} = \sqrt{\sum_{n=2}^{NN} \Delta \ell_n} \quad (5.6)$$

$$\text{cumulative anomaly difference} = \sqrt{\sum_{n=2}^{NN} \Delta c_n} \quad (5.7)$$

**Table 5.6** Limits of Four 10°x 10° Blocks where 1°x 1° Anomalies were set to Zero in Anomaly Set A.

#	Location	$\phi_N^{\circ} (\theta_i)$	$\phi_S^{\circ} (\theta_i)$	$\lambda_W^{\circ}$	$\lambda_E^{\circ}$	Remarks
1	Central Siberia	70 (20)	60 (29)	95	105	N. Hemisphere
2	Central Africa	20 (70)	10 (79)	25	35	N. Hemisphere
3	Southwest Africa	-10(100)	-20(119)	10	20	S. Hemisphere
4	Central Andes (S. America)	-20(120)	-30(129)	285	295	S. Hemisphere

By comparing the first two sets of columns in Table 5.5, we find noticeable changes in the coefficients when 200 1°x 1° anomalies are set to zero in the northern hemisphere in the anomaly set A. But the last two sets of columns in Table 5.5 show that the setting of 200 1°x 1° anomalies to zero in the southern hemisphere have the predominant effect. This is due to the average anomaly error estimate associated with the latitude band in which the anomaly is set to zero. With reference to Tables 5.6 and 4.1, the value of  $\sigma_i$  associated with the blocks in the northern hemisphere range from 16 to 14 and 10 to 7 mgals, while  $\sigma_i$  ranges from 7 to 8 and 4 to 5 mgals in the blocks in the southern hemisphere.

These tests highlight the importance of getting the best possible estimate (instead of zero) for the global anomalies, and assigning realistic standard errors to these estimates. The error estimates of 1°x 1° anomalies are, of course, averaged over each latitude band before these are utilized in the optimal estimation procedure.

#### 5.4 Improvement in Coefficients with Optimal Estimation

We now list in Table 5.7 the comparison of both coefficient sets A and B with optimally estimated coefficients to degree 180 from both anomaly sets A and B, using in each case anomaly error estimate A as well as anomaly error estimate B. By listing these comparisons side by side, we first note that only small differences exist in comparison with coefficient set A, when contrasted with comparisons made with coefficient set B, at lower degrees  $< 12$ ; coefficient sets A and B are, of course, exactly the same for degrees  $> 36$  (except for some coefficients to degree 48). We also note the slightly better agreement of coefficients estimated from anomaly set B, when contrasted with similar cases of coefficients estimated from anomaly set A, except at lower degrees  $< 24$ . The large disagreement at degrees 2 and 3 of optimally estimated coefficients from anomaly set B was commented upon in Section 5.2. The disagreement at degree 3 becomes worse for the anomaly error estimate A, as compared to anomaly error estimate B, because of the strong equatorial asymmetry of error estimate A in Table 4.1.

Besides other points already discussed in Sections 5.1 to 5.3, the improvement, particularly at higher degrees, in magnitude of coefficients estimated optimally instead of using the de-smoothing factors primarily results due to the consideration of realistic anomaly error estimates in optimal estimation, while the anomaly error estimates are not considered when de-smoothing factors are used. The current realistic

**Table 5.5** Variation of Optimally Estimated Coefficients with Variation in Global Anomaly Data.  
 Comparison of Coefficient Set A with 4 Coefficient Sets Estimated from 4 Global Anomaly Sets.  
 Anomaly Error Estimate A (Table 4.1) was used in all 4 cases.

Degree n	Anomaly Set A			Anomaly Set 1			Anomaly Set 2			Anomaly Set 3		
	% $\Delta\eta$	$\sqrt{\Delta\% \eta}$ m	$\sqrt{\Delta C \eta}$ mgal	% $\Delta\eta$	$\sqrt{\Delta\% \eta}$ m	$\sqrt{\Delta C \eta}$ mgal	% $\Delta\eta$	$\sqrt{\Delta\% \eta}$ m	$\sqrt{\Delta C \eta}$ mgal	% $\Delta\eta$	$\sqrt{\Delta\% \eta}$ m	$\sqrt{\Delta C \eta}$ mgal
2	.85	.15	.02	1.56	.28	.04	5.4	.97	.15	4.9	.87	.13
3	.40	.08	.02	.97	.18	.06	2.9	.55	.17	3.1	.59	.18
4	.44	.04	.02	1.33	.13	.06	4.3	.42	.19	4.9	.48	.22
6	.63	.04	.03	1.45	.08	.06	4.6	.26	.20	5.2	.30	.23
9	.67	.02	.02	2.5	.07	.08	7.6	.21	.25	8.4	.23	.28
12	1.4	.02	.03	5.2	.05	.09	14.6	.15	.26	15.1	.16	.27
24	3.9	.02	.06	8.4	.03	.12	21.4	.08	.30	24.1	.10	.34
36	5.0	.01	.07	8.4	.02	.11	23.2	.05	.29	24.4	.06	.31
48	6.6	.01	.11	5.5	.01	.08	20.9	.04	.32	22.0	.05	.34
60	6.9	.01	.13	3.5	.01	.06	17.8	.03	.31	17.8	.03	.31

Anomaly sets 1, 2, and 3 are alternations of Anomaly Set A (Section 4.1) by setting  $1^\circ \times 1^\circ$  anomalies to zero in  $10^\circ \times 10^\circ$  blocks as follows. Also see Figure 5.1 and Table 5.6.

- Set 1 : 2  $10^\circ \times 10^\circ$  blocks in N. hemisphere
- Set 2 : 2  $10^\circ \times 10^\circ$  blocks in S. hemisphere
- Set 3 : 4  $10^\circ \times 10^\circ$  blocks in N. and S. hemispheres

The total coefficient percentage error,  $\%T_n$ , per degree has been plotted in Figure 6.3 for both coefficient sets B1 and B2. Figure 6.3 has been reproduced from Rapp (1981, p. 33, Fig. 11) which showed  $\%T_n$  for the current coefficient set A.  $\%T_n$  had already reached 100% for coefficient set A at degree 120.  $\%T_n$  is better for sets B1 and B2 by more than a factor of two as compared to set A for all degrees greater than 12.

We may also examine the error estimates in undulation,  $\sigma_{\ell_n}$ , and anomaly,  $\sigma_{c_n}$ , per degree defined as:

$$\sigma_{\ell_n}^2 = R^2 \cdot \sigma_{\varepsilon_n}^2 = R^2 \cdot \sum_{m=0}^n (\sigma_{c_{nm}}^2 + \sigma_{s_{nm}}^2) \quad (6.4)$$

$$\sigma_{c_n}^2 = \gamma^2(n-1)^2 \cdot \sigma_{\varepsilon_n}^2 = \gamma^2(n-1)^2 \sum_{m=0}^n (\sigma_{c_{nm}}^2 + \sigma_{s_{nm}}^2) \quad (6.5)$$

and also cumulatively as  $\sqrt{\sum_n \sigma_{\ell_n}^2}$  and  $\sqrt{\sum_n \sigma_{c_n}^2}$  respectively. The undulation and anomaly error estimates, per degree, and cumulatively, have been tabulated in Table 6.4 for coefficient sets B1, B2, and also for the current coefficient set A.

We note that error estimates for sets B1 and B2 are better than a factor of two from the corresponding error estimates of set A for all degrees greater than 12. But the error estimates for sets B1 and B2 are much larger than those for set A at degree 6 and below, though as noted in Table 6.3, the coefficient percentage error itself for sets B1 and B2 is quite low at these degrees. This illustrates the well-known fact that the low degree potential coefficients can be estimated much better from satellite observations as compared to global anomaly data. The error estimates of low degree coefficients in set A have been put equal to the error estimates of 'adjusted SET1' coefficients (see Section 2.3), while the error estimates of sets B1 and B2 are based on the anomaly error estimates. If we were to assume that the error estimates for set B1 for degree  $\leq 6$  are taken from satellite observations, i.e. the same as for set A, then the cumulative undulation error for set B1 to degree 250 would become about 81 cm instead of 109 cm. In a similar way, the cumulative undulation error for set B2 to degree 250 would be reduced to about 56 cm instead of 67 cm. The cumulative undulation errors to degree 180 may then be compared for sets B1, B2 and A as about 75, 48 and 146 cm respectively. The error estimates in Table 6.4, and in the corresponding Figures 6.4 and 6.5, were however not changed.

The cumulative undulation error,  $\sqrt{\sum_n \sigma_{\ell_n}^2}$ , has been plotted for sets A, B1 and B2 as the top three curves in Figure 6.4. The undulation error,  $\sigma_{\ell_n}$ , per degree has also been plotted for set B1 as the bottom curve in Figure 6.4, except that the portion for degrees 3, 4, 5 has not been drawn in to avoid confusion.

The cumulative anomaly error,  $\sqrt{\sum_n \sigma_{c_n}^2}$ , has been plotted for the three sets A, B1, B2 in Figure 6.5, which also shows the anomaly error,  $\sigma_{c_n}$ , per degree for set B1 as the bottom curve.

**Table 6.4 Undulation and Anomaly Error Estimates per Degree and Cumulatively. Comparison of New and Current Sets of Potential Coefficients. Also, Variation Due to Anomaly Error Estimate on Optimally Estimated Coefficient Accuracies.**

Degree n	Coefficient Set B1				Coefficient Set B2				Coefficient Set A			
	Anomaly Error Estimate A				Anomaly Error Estimate B				Anomaly Errors (Section 2.3)			
	$\sigma^2_n$ cm	$\sqrt{\Sigma\sigma^2_n}$ cm	$\sigma C_n$ mgal	$\sqrt{\Sigma\sigma^2 C_n}$ mgal	$\sigma^2_n$ cm	$\sqrt{\Sigma\sigma^2_n}$ cm	$\sigma C_n$ mgal	$\sqrt{\Sigma\sigma^2 C_n}$ mgal	$\sigma^2_n$ cm	$\sqrt{\Sigma\sigma^2_n}$ cm	$\sigma C_n$ mgal	$\sqrt{\Sigma\sigma^2 C_n}$ mgal
2	50.7	51	.08	0.1	25.7	26	.04	0.0	1.6	1.6	.00	0.0
3	40.2	65	.12	0.1	22.2	34	.07	0.1	5.1	5.3	.02	0.0
6	18.7	76	.14	0.3	10.3	40	.08	0.2	10.9	18	.08	0.1
12	11.6	83	.20	0.5	6.4	44	.11	0.3	18.3	52	.31	0.7
24	7.7	89	.27	1.0	4.3	48	.15	0.5	14.2	77	.50	1.6
36	6.2	92	.33	1.4	3.5	50	.19	0.8	10.2	88	.55	2.5
60	4.8	96	.43	2.4	2.8	52	.25	1.3	11.9	109	1.08	5.3
90	4.1	98	.56	3.6	2.6	54	.36	2.2	9.7	124	1.33	8.5
120	3.9	101	.71	5.0	2.8	56	.51	3.2	8.6	134	1.57	11.7
150	3.8	103	.87	6.6	3.1	58	.70	4.6	7.7	141	1.77	14.9
180	3.8	105	1.03	8.4	3.3	61	.91	6.4	7.2	146	1.99	18.1
210	3.6	107	1.16	10.4	3.4	63	1.08	8.4				
240	3.4	109	1.25	12.3	3.2	66	1.19	10.5				
250	3.3	109	1.26	12.9	3.2	67	1.21	11.2				

Both coefficient sets B1 and B2 estimated from anomaly set B using anomaly error estimates A and B respectively. Error Estimate A :  $\sigma_j$  ranges from 30 to 4 mgals (Table 4.1); Error Estimate B :  $\sigma_j = 5$  mgals. Coefficient set A is the current set of coefficients (Rapp, 1981) to degree 180. (Also see Sec. 2.3).  $\sigma = 20$  mgals, but error of low degree coefficients based on satellite observations.

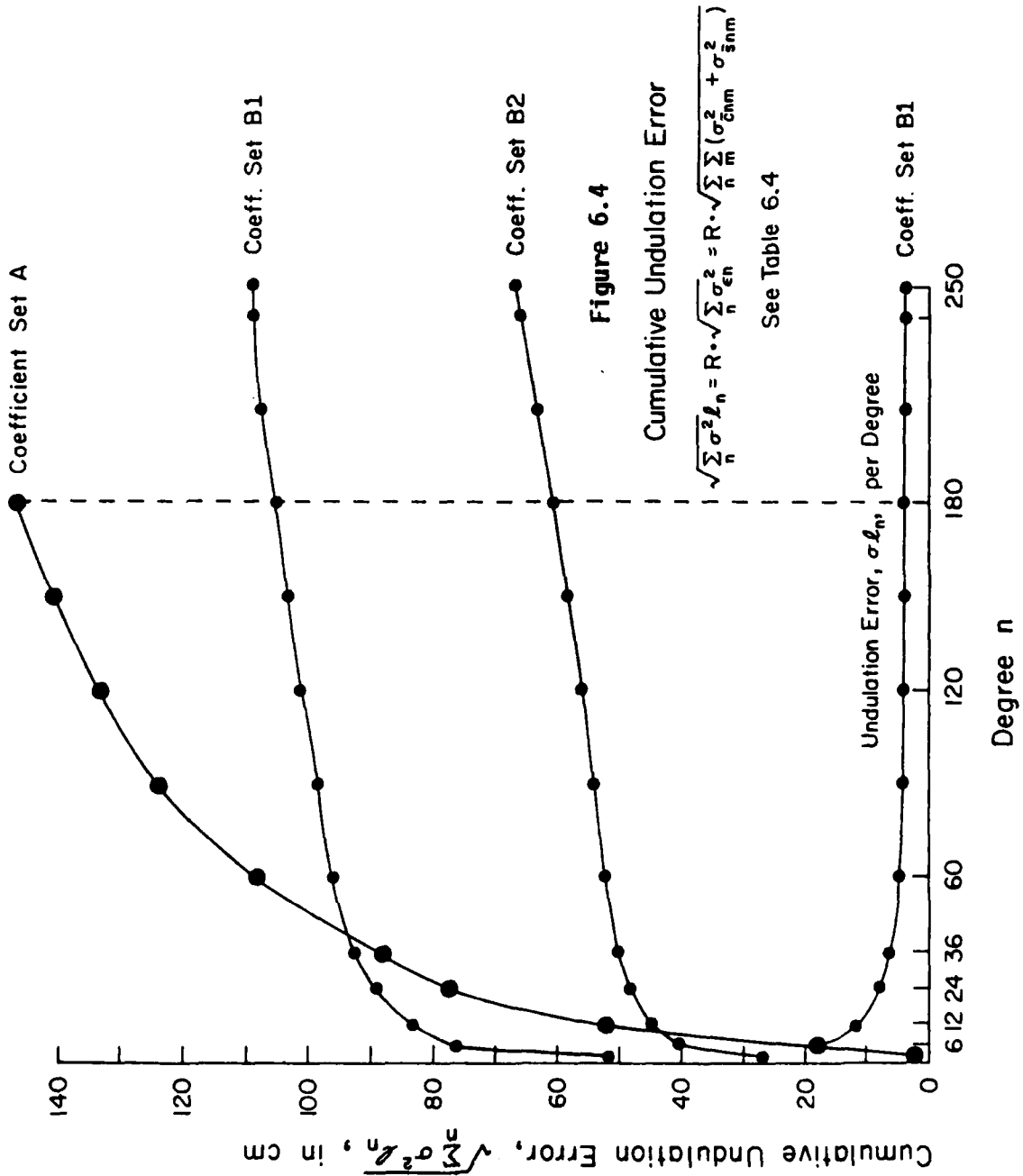
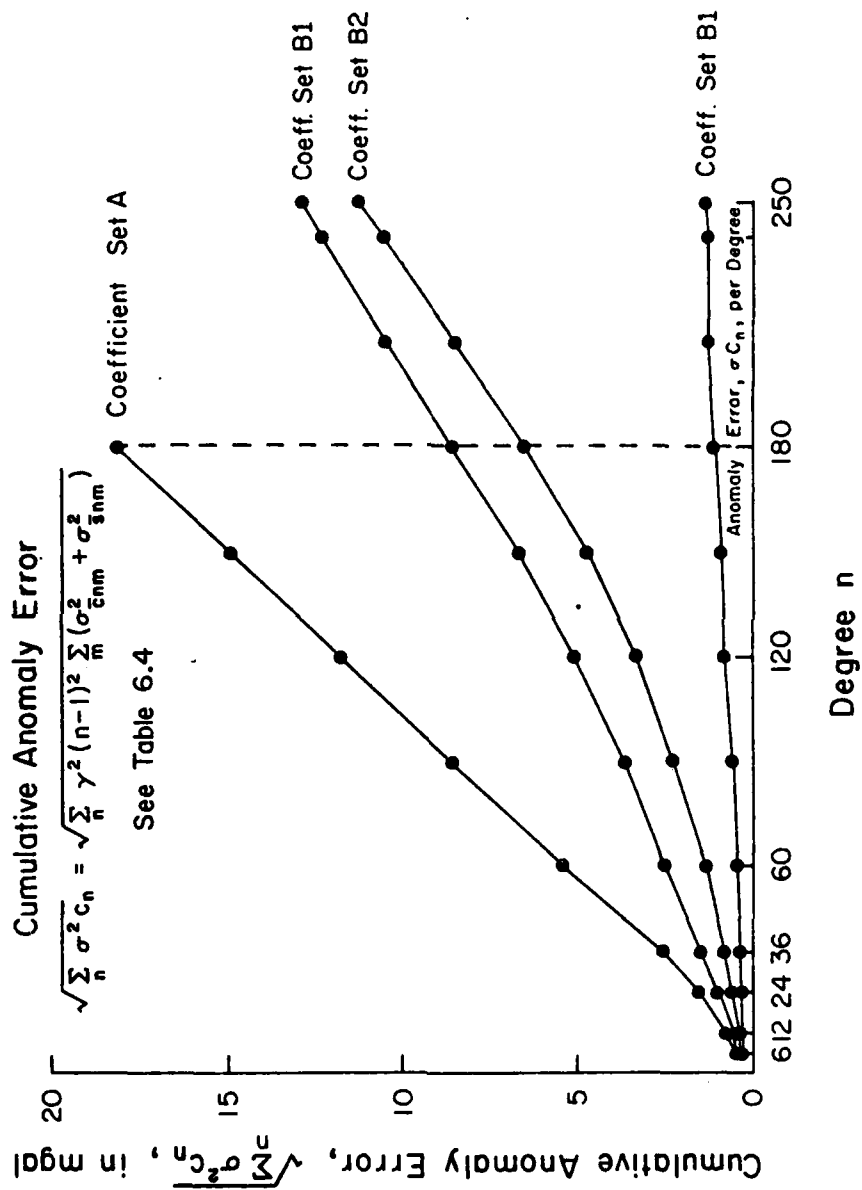


Figure 6.5



### 6.3 Empirical Anomaly Degree Variances

It is of interest to see what is the empirical anomaly degree variance  $\hat{c}_n$ , implied by the optimally estimated coefficient sets B1 and B2.

$$\hat{c}_n = \gamma^2(n-1)^2 \sigma_n^2; \quad \sigma_n^2 = \sum_{m=0}^n (\hat{C}_{nm}^2 + \hat{S}_{nm}^2) \quad (6.6)$$

Four sets of anomaly degree variances have been plotted in Figure 6.6. At the right edge of the plot, the curves in decreasing order of magnitude are: (1) the a-priori  $c_n$  model specified in (4.1) plotted with asterisks; (2) Kaula's model  $c_n^k$  corresponding to  $\sigma_n^k = 10^{-5}/n^2$  (Rapp, 1979, p. 1, (2)), which is the smooth curve in the plot; (3)  $\hat{c}_n$  for coefficient set B2; and (4)  $\hat{c}_n$  for coefficient set B1 plotted with crosses. As the optimal estimator in (2.19) in least squares collocation minimizes the sum of total variances for all coefficients, the larger the anomaly error estimate the smoother would be the optimally estimated coefficients. We accordingly find that  $\hat{c}_n$  for coefficient set B2 based on anomaly estimate B,  $\sigma_i = 5$  mgals, have consistently larger power as compared to coefficient set B1, based on larger anomaly error estimate A, with  $\sigma_i$  ranging from 30 to 4 mgals (Table 4.1).

We also note that the power in coefficient set B2 falls below Kaula's model for degrees higher than 200, while the a-priori  $c_n$  model has too much power for degrees higher than 150. These are indicative of both a need for slight downward adjustment of power in a-priori model in (4.1), and also that more reliable estimates for higher degrees would be obtained if the global anomaly data was available in blocks smaller than  $1^\circ \times 1^\circ$ .

Because of greater power in the a-priori model for  $c_n$ , the error estimates per degree are pessimistic at higher degrees, as larger error estimates are obtained from (3.8) with larger values of  $c_n$ . We have thus pessimistic undulation and anomaly error estimates per degree,  $\sigma_{\ell n}$  and  $\sigma_{c n}$  in Section 6.2, for higher degrees. On the other hand, the undulation and anomaly magnitude per degree,  $\sqrt{\ell_n}$  and  $\sqrt{c_n}$  in Section 6.1, decrease rapidly at higher degrees for coefficient set B1 due to large anomaly error estimate A. This explains why the signal to noise ratio appears to fall below 1 for coefficient set B1 for degrees 180 and higher, when we compare Tables 6.2 and 6.4. Similar results occur for coefficient set B2, which has more power than set B1, for degrees 200 and higher. This artifact however does not occur in Table 6.3 and Figure 6.3, where the coefficient percentage error does not exceed 85% even at degree 250. This is due to the percentage errors being computed through (6.2) and (6.3), where the numerator and denominator both depend on the a-priori  $c_n$  model.

We next compare  $\hat{c}_n$  implied by coefficient sets B1 and B2, with  $\hat{c}_n$  implied by the current coefficient set (Rapp, 1981), i.e. coefficient set A computed with de-smoothing factors (2.7) but we now consider the latter set also up to degree 250, including the sharp discontinuity at degree 180.  $\hat{c}_n$  values are compared for coefficient sets B2 and A in Figure 6.7; and for coefficient sets B1 and A in Figure 6.8. The curves for coefficient set A are plotted with asterisks

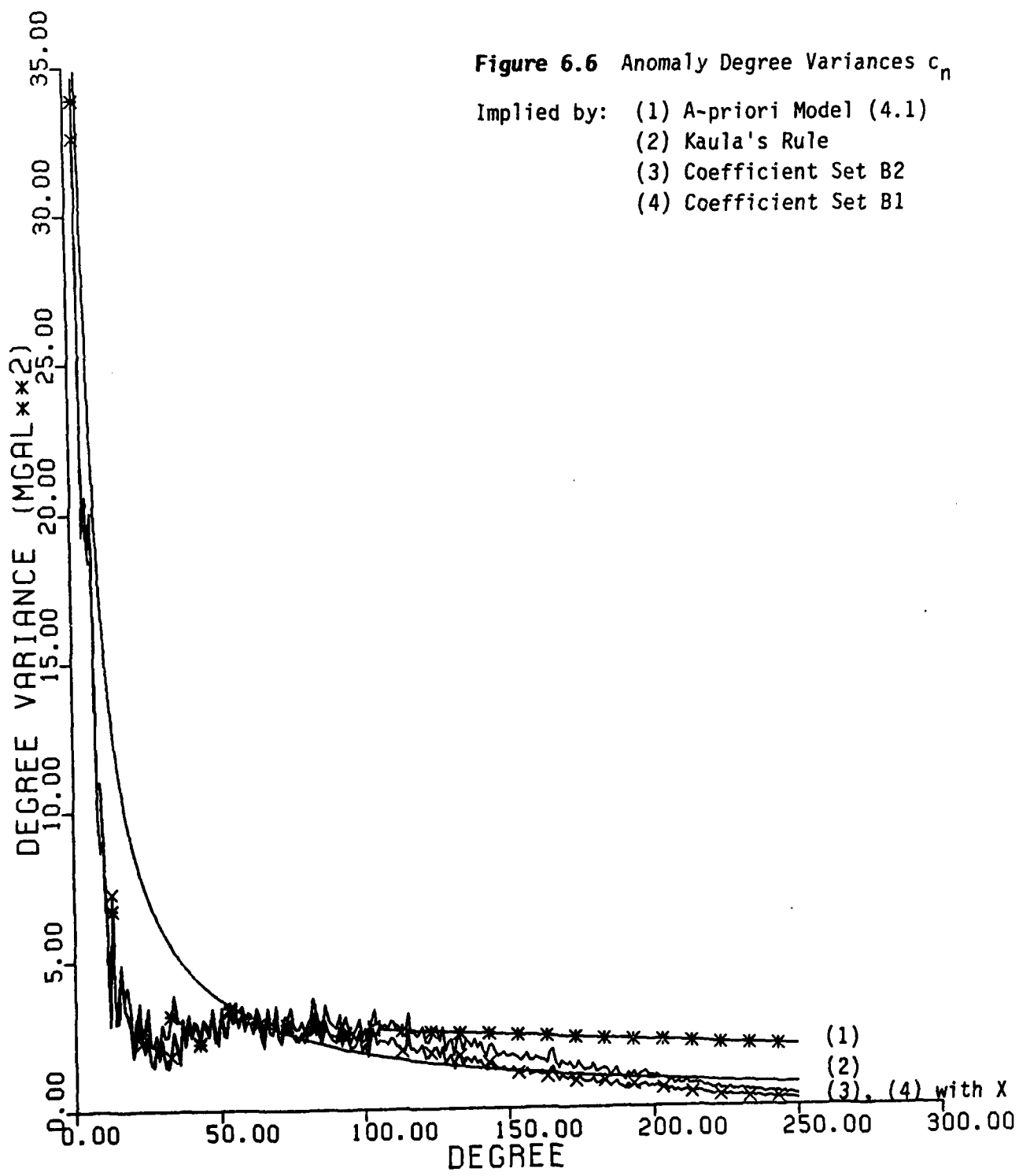
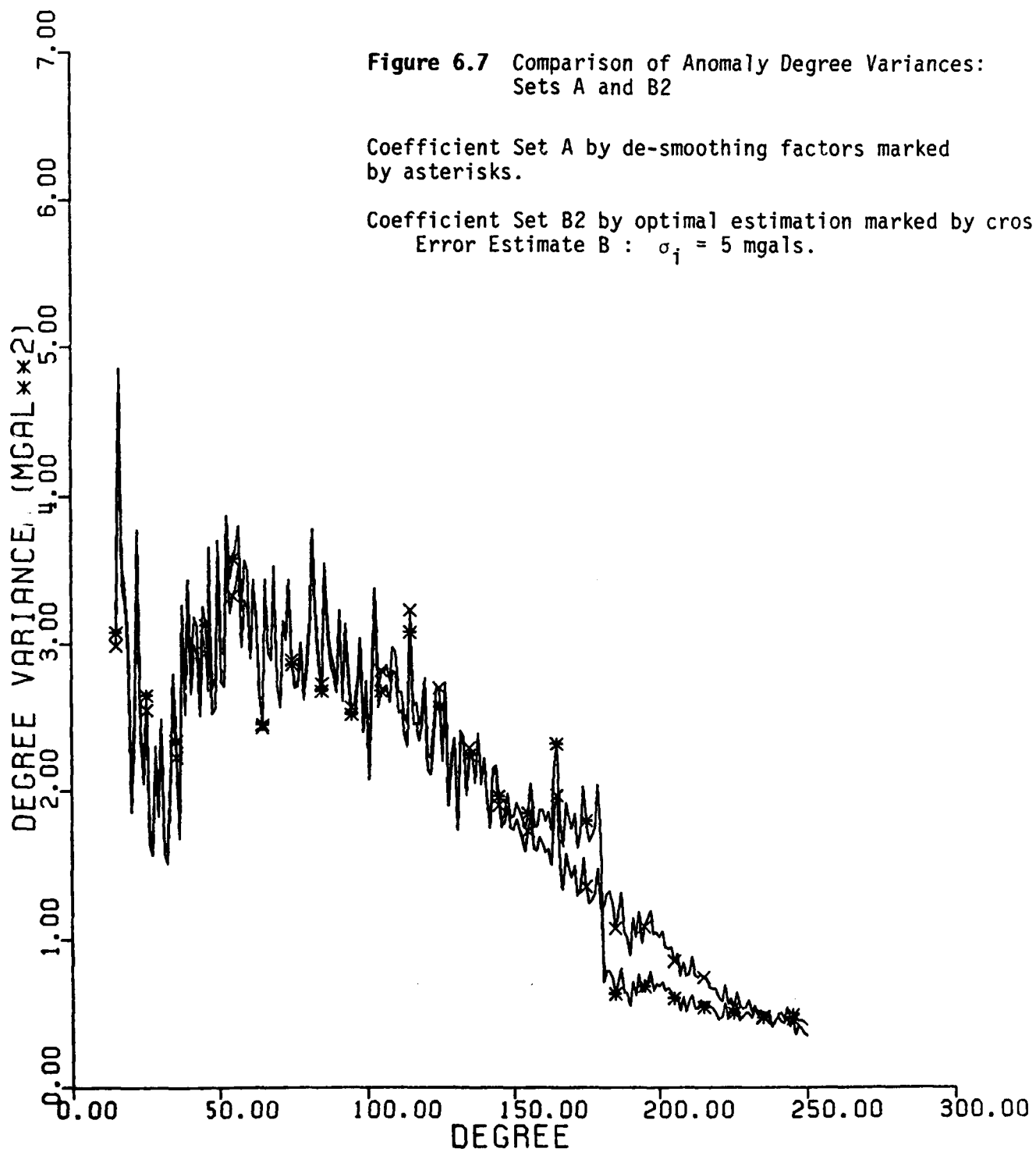


Figure 6.6 Anomaly Degree Variances  $c_n$

- Implied by: (1) A-priori Model (4.1)  
 (2) Kaula's Rule  
 (3) Coefficient Set B2  
 (4) Coefficient Set B1

in both figures, while the curves for coefficient sets B2 and B1 are plotted with crosses. The scale of  $\hat{c}_n$  in Figures 6.7 and 6.8 is exaggerated five times as compared to Figure 6.6.

The sharp discontinuity at degree 180 for coefficient set A is clearly seen in Figures 6.7 and 6.8. The smaller discontinuity at degree 60 may be inferred in Figure 6.7, where the curve with asterisks (coefficient set A) has more power for  $n < 60$ , and lesser power for  $n > 60$  as compared to curve with crosses (coefficient set B2). Except for the sharp discontinuity at degree 180, the spectrums of coefficient sets A and B2 are fairly close in Figure 6.7, i.e. when we do not consider any latitudinal variation in anomaly error estimate B for the optimal estimation of coefficient set B2. However, when we do consider the currently realistic latitudinal variations in anomaly error estimate A for the optimal estimation of coefficient set B1, the spectrums of sets B1 and A differ substantially in Figure 6.8 for the entire range.

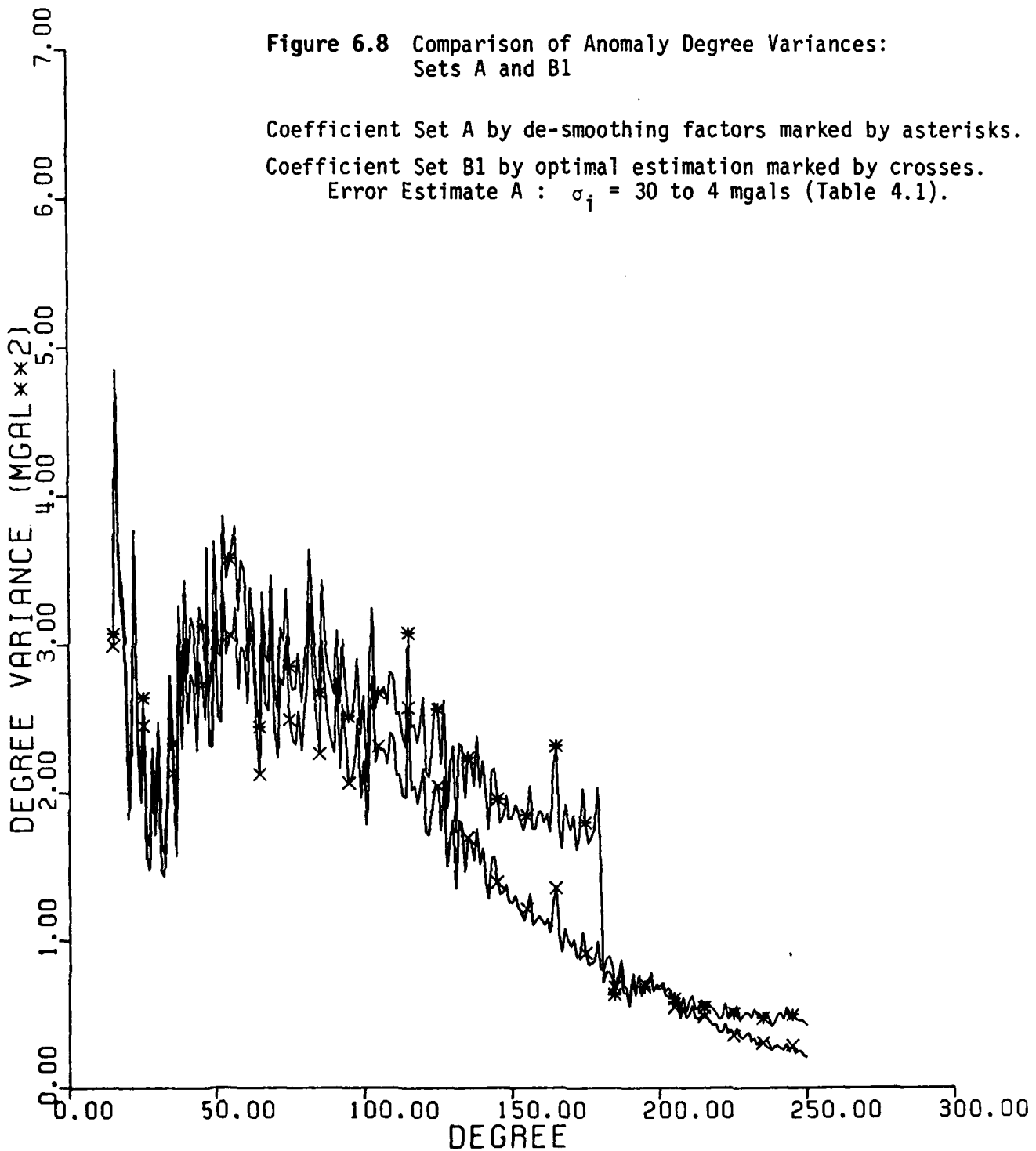


**Figure 6.8 Comparison of Anomaly Degree Variances:  
Sets A and B1**

Coefficient Set A by de-smoothing factors marked by asterisks.

Coefficient Set B1 by optimal estimation marked by crosses.

Error Estimate A :  $\sigma_i = 30$  to 4 mgals (Table 4.1).



## 7. SUMMARY AND CONCLUSIONS

The present study extends the algorithm developed by Colombo (1981), and tested with  $5^\circ \times 5^\circ$  anomalies, to the use of  $1^\circ \times 1^\circ$  anomalies globally for the optimal estimation of a high degree potential coefficients field, complete to degree and order 250, along with their error estimates. The algorithm was divided into several steps, for ease of computer implementation and running various tests, and also needed two main modifications. These steps have been summarized in Table 3.4.

The initial first step is to assemble the integrals of associated Legendre functions in  $1^\circ$  latitude bands by an efficient algorithm to a degree  $N_{\max}$ , which should be larger than the highest degree NN to which coefficients will be estimated and smaller than  $(2\pi/\text{anomaly block size})$ , i.e. 360. A total of  $(N_{\max}+1)(N_{\max}+2)/2$  integrals, which comes to 45,451 for  $N_{\max}=300$ , need to be computed for each  $1^\circ$  latitude band. The integrals are modified by factors, depending on the anomaly degree variances and the anomaly block size, for later processing. The anomaly degree variance model in (4.1) was used, which is the current global model.

The generation of normals, which are based on combinations of the Fourier transforms of the modified integrals in the first step for different pairs of latitude bands, could take large CPU time depending on degree NN. The two main modifications to the algorithm, i.e. the reordering of the normals and the reordering of the right hand side vectors, became necessary due to very large TAPE IO and array size requirements for the case of  $1^\circ \times 1^\circ$  anomalies. These two modifications, which are described in Sections 3.31 and 3.32, also depend on degree NN. As none of the steps so far depend on anomaly errors, or anomalies, different tests were carried out as described in Section 5 with NN=12 or 60.

The solution of normals, yielding the optimal quadrature weights, and the computation of error estimates, depends on the anomaly error estimates. An averaged variance is used in each latitude band, based on the anomaly error estimates in that latitude band, as discussed in Section 2.2 to allow the inversion of covariance matrix of 64,800  $1^\circ \times 1^\circ$  anomalies to be equivalently carried out by the inversion of  $180 \times 180$  matrices in the frequency domain to degree NN. The use of averaged anomaly variance in each latitude band allows the correct computation of only the sum of variances for the two coefficients ( $\bar{C}_{nm}$ ,  $\bar{S}_{nm}$ ) for any particular degree and order, and not separate variance for each coefficient in the pair. The variance for each coefficient in the pair is then arbitrarily made equal.

A very realistic anomaly error estimate, given in Table 4.1, was used for solution to degree NN=250. Because only an averaged variance is required in each latitude band, the anomaly error model is primarily sensitive to latitude variation. Accordingly, another solution of the normals was done to degree NN=250 with an anomaly error estimate without any latitude variation. The two anomaly error estimates, one in Table 4.1 with average anomaly error in a latitude band ranging from 30 to 4 mgals, and the other with a uniform value of 5 mgals in all latitude bands, were called anomaly error estimates A and B.

The computation of potential coefficients is the last step, where the global anomaly data is used with the optimal quadrature weights, which are dependent on the anomaly error estimates. The current best estimate of a global  $1^\circ \times 1^\circ$  anomaly field, anomaly set B adjusted to a weighted set of satellite derived potential coefficients 'SET1' complete to degree 36, with some additional coefficients to degree 48, was described in Section 2.3. Anomaly set B was used with anomaly error estimates A and B to compute potential coefficient sets B1 and B2 complete to degree and order 250. The statistics on these two coefficient sets, and the comparison with the current set of potential coefficients, coefficient set A, complete to degree and order 180 (Rapp, 1981), was presented in Section 6.

When the next updated version of a global set of  $1^\circ \times 1^\circ$  anomalies is assembled, it will be necessary to only repeat the last step of the computation of an updated set of potential coefficients. The latitude variations of the averaged anomaly variances in anomaly error estimate A are unlikely to change in the near future till the flight of the Geopotential Research Mission. The optimal quadrature weights corresponding to anomaly error estimate A, (and those corresponding to anomaly estimate B with no latitude variation of anomaly errors), of this study would therefore be directly usable with an updated version of global  $1^\circ \times 1^\circ$  anomalies.

#### 6.1 Conclusions of Present Study

- The most reliable estimate should be used for the global gravity anomaly data. When no reliable  $1^\circ \times 1^\circ$  anomaly estimates are available, the anomaly implied by a high degree potential coefficients field should be used in preference to setting the anomaly estimate as zero. The lower the averaged variance of anomalies in a  $1^\circ$  latitude band, the larger is the effect of change in anomaly estimate for any  $1^\circ \times 1^\circ$  anomaly in that latitude band.

- The most realistic error estimate should be used for each anomaly, instead of using a global average. Though the anomaly variances are averaged in each  $1^\circ$  latitudinal band before their introduction in optimal estimation of coefficients, the potential coefficient determination is quite sensitive to any resulting latitude variation of averaged variances in each  $1^\circ$  latitude band.

- The optimal quadrature weights,  $x_{nm}^i$ , are computed as 180 numbers for each specific coefficient pair,  $(\bar{C}_{nm}, \bar{S}_{nm})$ , of given degree and order. The 180 numbers take into account the latitudinal variation of averaged anomaly variances. The de-smoothing factors are based on the Pellinen/Meissl smoothing operator,  $\beta_n$ , which is the same for all orders for a given degree. Further, the de-smoothing factors do not take account of any anomaly error estimates, or more specifically any latitudinal variation in these estimates.

- The optimal quadrature weights are computed based on the minimization of the propagated anomaly error variances, and the error variance due to sampling a finite number of mean anomalies, instead of an infinite number of point anomalies. The desmoothing factors are based only on the size of anomaly blocks.

- The order of improvement in the coefficients, per degree, by optimal estimation over the current estimates using de-smoothing factors, is about 8% at degree 60, about 11% at degree 120, and rises to about 33% at degree 180.

- The error estimates in optimal estimation are consistent with anomaly error estimates in a meaningful way. The total percentage error,  $\%T_n$ , per degree does not exceed 100% even at degree 250.  $\%T_n$  had exceeded 100% for current set of coefficients at degree 120.

- The error estimates per degree in optimal estimation are better than a factor of two over the corresponding estimates in the current set of coefficients for all degrees greater than 12. The error estimates for low degrees in current coefficients are based on satellite observations, while the error estimates per degree in optimal estimation are based only on anomaly data.

- If the error estimates per degree in optimal estimation procedure are set to the same values as current coefficient set only for degrees  $\leq 6$ , the cumulative undulation error to degree 180 would be 75 cm as compared to 146 cm for current set of coefficients.

- There is no discontinuity in the degree variances of optimally estimated coefficients at degrees 60 and 180, as is the case with the current set of coefficients, which were limited to degree 180 because of concern over sharp discontinuity at that degree.

- No useful purpose may be served by expanding  $1^\circ \times 1^\circ$  gravity anomaly data into coefficients beyond degree 250. The undulation and anomaly magnitude per degree near  $n=250$  is about 1 cm and 0.5 mgals respectively. The coefficient percentage error near  $n=250$  exceeds 80%.

- The a-priori anomaly degree variance model has too much power beyond degree 50. This leads to pessimistic error estimates per degree, and cumulatively, at higher degrees.

## 2. Recommendations for Further Investigations

- The optimal estimation algorithm applied to  $1^\circ \times 1^\circ$  anomaly data needs to be extended further to consider the case when global anomaly data may be available in  $30' \times 30'$  blocks. Efforts have already been initiated (private communication from R.H. Rapp) to assemble a global data of 259,200  $30' \times 30'$  anomalies. This will lead to several fold increase in the complexity of computer implementation of the optimal estimation algorithm.

- The generation of normals requires  $(N_{max}+1)(N_{max}+2)/2$  integrals of associated Legendre functions to be read in for each latitude band to obtain Fourier transform of the data in a pair of latitude bands. Even after exploiting the persymmetric structure of the normals matrix, about 136,000 TAPE IO's are required only to read in the data from all required pairs of latitude bands for  $N_{max}=300$  for  $1^\circ$  latitude bands. It needs to be investigated if data from several pairs of latitude bands could be operated upon simultaneously instead of one pair at a time. Efficiency of putting part of this data on random storage also needs to be considered.

- The CPU time for the solution of normals increases sharply with increase in the highest degree to which coefficients are estimated. At degree 250, the solution of normals in sequence of right hand side vectors after inverting matrices of only  $180 \times 180$  for the case of  $1^\circ \times 1^\circ$  anomalies already took about 4 minutes CPU time on an Amdahl 470 V/8 computer. Faster algorithms need to be investigated for this solution.

- Bose et al. (1983) have suggested some strategies for including data at poles but the computational load does not decrease significantly. They have suggested different data sampling instead of equi-angular blocks. Further investigations need to be continued to apply such strategies to actual computations high degree field.

## References

- , S.C., G.E. Thobe, J.T. Kouba and R.W. Mortensen, Optimal Global Gravity Representation, Paper presented at the XVIII General Assembly of IUGG, Proc. of IAG Symposia, Vol. 1, pp. 449-482, Hamburg, August 1983.
- nbo, O.L., Optimal Estimation from Data Regularly Sampled on a Sphere with Applications in Geodesy, Department of Geodetic Science Report No. 291, The Ohio State University, Columbus, September 1979.
- nbo, O.L., Numerical Methods for Harmonic Analysis on the Sphere, Department of Geodetic Science and Surveying, Report NO. 310, The Ohio State University, Columbus, March 1981.
- tl, M., On the Recursive Computation of the Integrals of the Associated Legendre Functions, Manuscripta Geodaetica, Vol. 5, pp. 181-199, 1980.
- son, D.M., On Solving the Stability Problem in Computing the Integrals of the Legendre Functions, Department of Geodetic Science and Surveying Internal Report, The Ohio State University, Columbus, August 1983.
- h, F.J., B.J. Putney, C.A. Wagner and S.M. Klosko, Goddard Earth Models for Oceanographic Applications (GEM 10B and 10C), Marine Geodesy, Vol. 5, No. 2, pp. 145-187, 1981.
- tz, H., Advanced Physical Geodesy, Abacus Press, Kent, U.K., 1980a.
- tz, H., Geodetic Reference System 1980, Bulletin Geodesique, Vol. 54, No. 3, pp. 395-405, 1980b.
- , M.K., Recurrence Relations for Integrals of Associated Legendre Functions, Bulletin Geodesique, Vol. 52, pp. 177-190, 1978.
- i, R.H., Analytical and Numerical Differences Between Two Methods for the Combination of Gravimetric and Satellite Data, Boll. di Geof. Teo. ed Appl., Vol. XI, N41-42, pp. 108-118, 1979.
- i, R.H., The Relationship Between Mean Anomaly Block Sizes and Spherical Harmonic Representations, Journal of Geophysical Research, Vol. 82, No. 33, pp. 5360-5364, November 1977.
- i, R.H., Potential Coefficient and Anomaly Degree Variance Modeling Revisited, Department of Geodetic Science and Surveying Report No. 293, The Ohio State University, Columbus, September 1979.
- i, R.H., The Earth's Gravity Field to Degree and Order 180 Using Seasat Altimeter Data, Terrestrial Gravity Data, and Other Data, Department of Geodetic Science and Surveying Report No. 322, The Ohio State University, Columbus, December 1981.
- i, R.H., Aspects of Geoid Definition and Determination, Proc. of the General Meeting of the IAG, pp. 411-433, Tokyo, May 1982.

Tscherning, C.C., The Role of High Degree Spherical Harmonic Expansions in Solving Geodetic Problems, Paper presented at the XVIII General Assembly of IUGG, Proc. of IAG Symposia, Vol. 1, pp. 431-441, Hamburg, August 1983.

Tscherning, C.C., R.H. Rapp and C.C Goad, A Comparison of Methods for Computing Gravimetric Quantities from High Degree Spherical Harmonic Expansions, Manuscripta Geodaetica, Vol. 8, pp. 249-272, 1983.

**END**

**FILMED**

**8-85**

**DTIC**